Promotional issue

INTERFACE FOCUS

Carbon dioxide detection in biological systems

Theme issue organized by Victoria L. Linthwaite, Eoin Cummins and Martin J. Cann

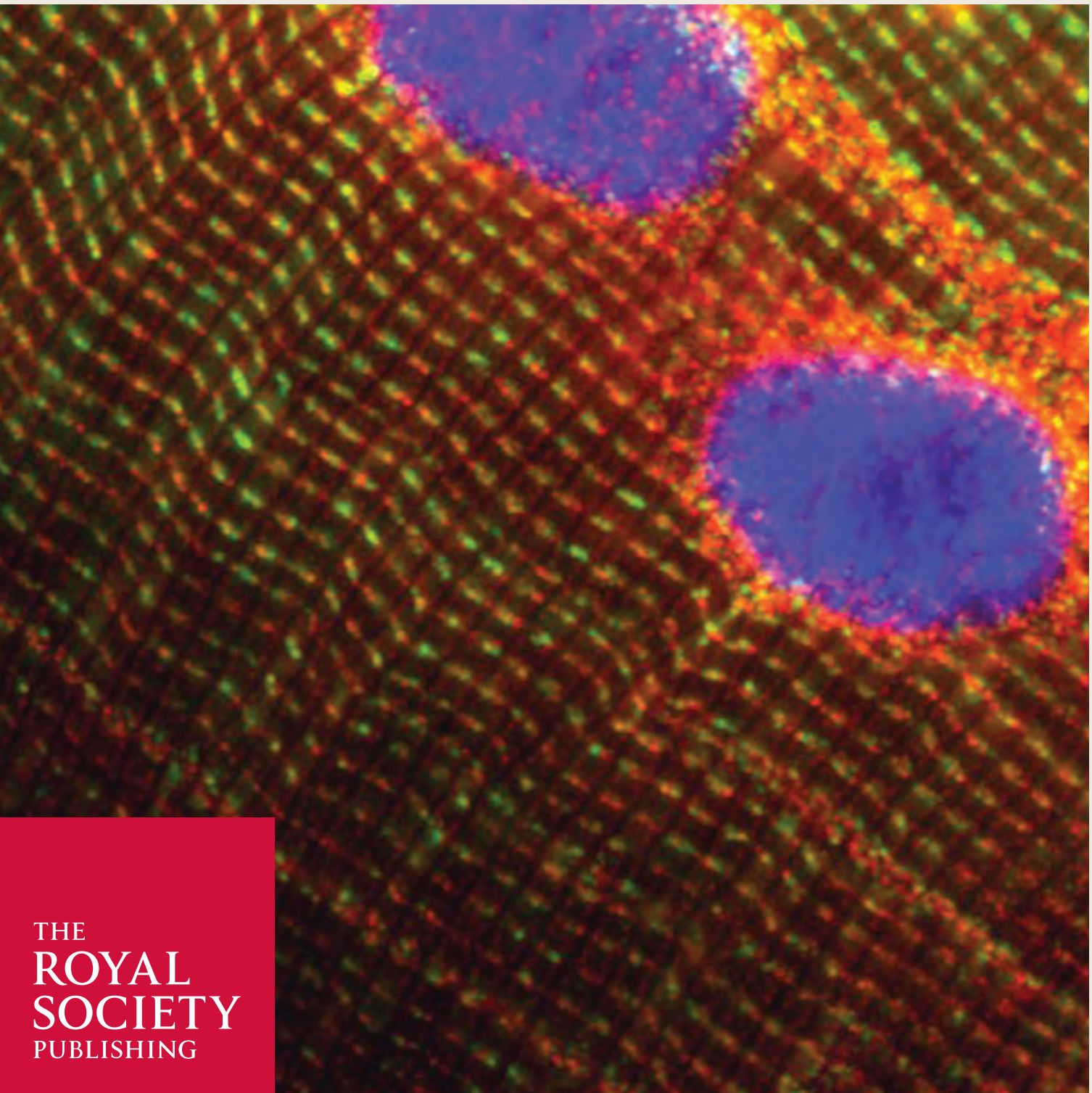

THE ROYAL SOCIETY PUBLISHING

Cover image
White muscle fibre from rainbow trout abundantly express the enzyme soluble adenylyl cyclase (sAC, in red), which is found in close association with actin (in green) and with nuclei (in red). Since sAC is an evolutionary conserved carbon dioxide, pH and bicarbonate molecular sensor, it might play important roles in muscle physiology. The image was obtained using immunostaining and confocal super-resolution microscopy. (Image credit: Garfield Kwan, Till Harter, Martin Tresguerres; see the article 'Molecular and biochemical characterization of the bicarbonate-sensing soluble adenylyl cyclase from a bony fish, the rainbow trout *Oncorhynchus mykiss*' (https://doi.org/10.1098/rsfs.2020.0026) published in this issue).

Typeset in India by Nova Techset Private Limited, Bengaluru & Chennai, India. Printed in the UK by Cambrian Printers.

This paper meets the requirements of ISO 9706:1994(E) and ANSI/NISO Z39.48-1992 (Permanence of Paper).

INTERFACE FOCUS

royalsocietypublishing.org/journal/rsfs

Research

Cite this article: Salmerón C *et al*. 2021 Molecular and biochemical characterization of the bicarbonate-sensing soluble adenylyl cyclase from a bony fish, the rainbow trout *Oncorhynchus mykiss*. *Interface Focus* **11**: 20200026.
https://doi.org/10.1098/rsfs.2020.0026

Accepted: 9 December 2020

One contribution of 13 to a theme issue 'Carbon dioxide detection in biological systems'.

Subject Areas:
biochemistry, environmental science, biocomplexity

Keywords:
cAMP, CO_2, Golgi, microdomain, pH sensing, sAC

Author for correspondence:
Martin Tresguerres
e-mail: mtresguerres@ucsd.edu

Electronic supplementary material is available online at https://doi.org/10.6084/m9.figshare.c.5260354.

THE ROYAL SOCIETY PUBLISHING

Molecular and biochemical characterization of the bicarbonate-sensing soluble adenylyl cyclase from a bony fish, the rainbow trout *Oncorhynchus mykiss*

Cristina Salmerón[1,2], Till S. Harter[1], Garfield T. Kwan[1], Jinae N. Roa[1], Salvatore D. Blair[3,4], Jodie L. Rummer[5], Holly A. Shiels[6], Greg G. Goss[3], Rod W. Wilson[7] and Martin Tresguerres[1]

[1]Scripps Institution of Oceanography, University of California San Diego, La Jolla, CA, USA
[2]Department of Pharmacology, University of California San Diego, San Diego, CA, USA
[3]Department of Biological Sciences, University of Alberta, Edmonton, Alberta, Canada
[4]Department of Biology, Winthrop University, Rock Hill, SC, USA
[5]Australian Research Council Centre of Excellence for Coral Reef Studies, James Cook University, Townsville, Queensland, Australia
[6]Division of Cardiovascular Sciences, Faculty of Biology, Medicine and Health, University of Manchester, UK
[7]Department of Biosciences, University of Exeter, Exeter, UK

MT, 0000-0002-7090-9266

Soluble adenylyl cyclase (sAC) is a HCO_3^--stimulated enzyme that produces the ubiquitous signalling molecule cAMP, and deemed an evolutionarily conserved acid–base sensor. However, its presence is not yet confirmed in bony fishes, the most abundant and diverse of vertebrates. Here, we identified sAC genes in various cartilaginous, ray-finned and lobe-finned fish species. Next, we focused on rainbow trout sAC (rtsAC) and identified 20 potential alternative spliced mRNAs coding for protein isoforms ranging in size from 28 to 186 kDa. Biochemical and kinetic analyses on purified recombinant rtsAC protein determined stimulation by HCO_3^- at physiologically relevant levels for fish internal fluids ($EC_{50} \sim 7$ mM). rtsAC activity was sensitive to KH7, LRE1, and DIDS (established inhibitors of sAC from other organisms), and insensitive to forskolin and 2,5-dideoxyadenosine (modulators of transmembrane adenylyl cyclases). Western blot and immunocytochemistry revealed high rtsAC expression in gill ion-transporting cells, hepatocytes, red blood cells, myocytes and cardiomyocytes. Analyses in the cell line RTgill-W1 suggested that some of the longer rtsAC isoforms may be preferentially localized in the nucleus, the Golgi apparatus and podosomes. These results indicate that sAC is poised to mediate multiple acid–base homeostatic responses in bony fishes, and provide cues about potential novel functions in mammals.

1. Background

The enzyme soluble adenylyl cyclase (sAC, *adcy10*) is directly stimulated by bicarbonate ions (HCO_3^-) to produce the ubiquitous messenger molecule cyclic adenosine monophosphate (cAMP) [1]. In the presence of carbonic anhydrase (CA), carbon dioxide (CO_2), proton (H^+) and HCO_3^- are in a near instantaneous equilibrium, and this enables sAC to act as a general acid–base sensor for multiple physiological processes (reviewed in [2,3]).

The original biochemical studies in the 1970s reported a 'soluble' source of cAMP in rat testes that was distinct from the traditional transmembrane ACs (tmACs) based on the potent stimulation induced by Mn^{2+} and its insensitivity

to hormones and fluoride [4,5]. However, it took about 20 years until the Mn^{2+}-stimulated AC enzyme was finally identified as sAC [6]. It was simultaneously discovered that the two catalytic domains of sAC, C1 and C2, were more similar to ACs from cyanobacteria than to the tmACs that first appeared in metazoans, indicating that sAC is an evolutionarily conserved enzyme [6]. Shortly after, sAC activity was found to be directly stimulated by HCO_3^- [1], which led to a flurry of studies on its potential role as an acid–base sensor in diverse organisms. Initially, the lack of sAC genes in the genomes of *Drosophila* and *Caenorhabditis elegans* was interpreted as evidence that sAC had been lost in most animal phyla [7]; however, the subsequent identification and characterization of sAC in sea urchin [8], shark [9] and coral [10] confirmed that sAC indeed is an evolutionarily conserved acid–base sensing enzyme.

The stimulating effect of HCO_3^- on the activity of sAC is species-specific. In mammalian sAC, the HCO_3^- half maximal stimulation (EC_{50}) is approximately 20 mM [1,11,12], whereas that of shark sAC is only approximately 5 mM [9]; and these values closely match average HCO_3^- concentrations in the internal fluids of these organisms. As a result, cAMP production by sAC is maximally modulated by small HCO_3^- fluctuations around species-specific homeostatic set points [13,14]. In addition, *in vitro* characterization of sAC cAMP-producing activity revealed a potent stimulation by millimolar [Mn^{2+}] (reviewed in [15]). However, the physiologically relevant catalytic metals that sustain HCO_3^- stimulation *in vivo* are Mg^{2+} and Ca^{2+} for mammalian sAC [12], and Mg^{2+} and Mn^{2+} for shark sAC [9]. Advances from pharmacological studies have provided essential tools for studying sAC activity *in vivo*. Both mammalian and shark sACs are inhibited by derivatives of catechol estrogen (dCE) and by the small molecules KH7 and LRE1 [9,16–19], and are insensitive to the widely used tmAC stimulator, forskolin, and to the tmAC inhibitor, 2,2-dideoxyadenosine (DDA) [16,20]. Other work has described the presence of numerous alternative promoters in the sAC gene as well as extensive alternative splicing, which have been characterized to different extents in some mammals [21–25], corals [10] and sharks [26].

As a result of the most expansive adaptive radiations among vertebrates, ray-finned fishes (Actinopterygii) make up half of all vertebrates on Earth and are of great ecological and economical importance. As is typical for water-breathing animals, fishes may routinely experience severe acid–base disturbances such as exercise-induced acidosis, postprandial alkaline tide and environmental hypercapnia that can induce large fluctuations in plasma [HCO_3^-] ranging nearly 0 to over 50 mM (reviewed in [27,28]). Although sAC is an ideal candidate to sense acid–base disturbances and trigger compensatory responses in ray-finned fishes, the apparent absence of sAC genes in the zebrafish, puffer fish and medaka genomes initially suggested that sAC had been lost in ray-finned fishes, and that they may use fundamentally distinct mechanisms for acid–base sensing [9]. However, the apparent absence of sAC genes in teleost fishes could be explained by the high structural complexity of the sAC gene that may confound its identification using bioinformatics tools (reviewed in [15]). Indeed, the presence of sAC in ray-finned fishes is supported by sAC-like immunoreactivity in the intestine of the toadfish (*Opsanus beta*) [29], in Atlantic salmon (*Salmo salar*) sperm [30], and in Pacific chub mackerel (*Scomber japonicus*) inner ear epithelium [31]. Furthermore, the reported sensitivity of NaCl and water absorption in the intestine of marine fish to pharmacological inhibitors of sAC [29,32] provided functional evidence for its presence. More recently, partial sAC coding sequences were identified by BLAST searches in gar, rainbow trout and salmon [14]. However, a detailed molecular and biochemical characterization of sAC genes and proteins from ray-finned fishes is still absent, which is currently hindering functional studies about the roles of sAC.

Therefore, in the current study, we explored and identified nucleotide sequences coding for sAC in genomic and transcriptomics databases from multiple ray-finned fish species. Of those, we focused on sAC from the rainbow trout (*Oncorhynchus mykiss*), a teleost fish that is widely used as a model species for physiological, ecological and applied studies in aquaculture. Subsequently, we: (i) cloned multiple rainbow trout sAC (rtsAC) variants, (ii) characterized the enzymatic activity of recombinant purified rtsAC protein, and (iii) determined the presence and subcellular localization of rtsAC in different tissues. The novel molecular, biochemical and immunocytochemical findings of this study provide a solid foundation for future functional studies and will enable investigating the role of sAC as an acid–base sensor in ray-finned fishes.

2. Methods

2.1. Experimental animals

Oncorhynchus mykiss were maintained in freshwater aquaria at the Bamfield Marine Science Center (BC, Canada), the Aquatic Resources Centre at University of Exeter (UK), or the University of Manchester (UK). Procedures were approved by animal care protocols from the University of Alberta (AUP00001126 and AUP00000072), University of Exeter (PPL P88687E07), and University of Manchester (HO lic 40/3584). After euthanasia, samples were stored at −80°C, in RNA*later*, or in fixative for immunostaining (see electronic supplementary material for more details).

2.2. Bioinformatics and cloning of rtsAC splice variants

Phylogenetic analysis was performed using Phylogeny.fr with 100 bootstraps (http://www.phylogeny.fr/) [33] (electronic supplementary material, figure S1). Protein domains, tetratricopeptide repeat (TPR) motifs and intracellular targeting sequences were, respectively, identified on NCBI's Conserved Domain Database, TPRpred (https://toolkit.tuebingen.mpg.de/#/tools/tprpred), and the ngLOC database (http://genome.unmc.edu/ngLOC/index.html). Cloning was performed on purified mRNA from trout testis and RTgill-W1 cells using standard techniques. Primers included $Oligo(dT)_{20}$ and 2 µM gene-specific primers (electronic supplementary material, table S1). RT-PCR was performed using Phusion High-Fidelity PCR Master Mix (New England Biolabs, Ipswick, MA, USA). PCR products were purified and cloned into pCR 2.1 TOPO vectors (Thermo Fisher Scientific). Plasmids were heat-shock transformed into One Shot TOP10 Chemically Competent *E. coli* cells (Thermo Fisher Scientific), purified and sequenced using M13 (-20) FW, M13 RV or rtsAC-specific primers. The exon organization, splicing mechanisms, and other features of the cloned rtsAC isoforms are shown in electronic supplementary material, figure S3.

2.3. Production of recombinant rtsAC

The cDNA coding for a 53 kDa rtsAC protein (GenBank no. MF034901, named as $rtsAC_T$; see Results) was cloned into pDEST17 thus adding a 6X His-tag at the N-terminus

(His-rtsAC$_T$). Plasmids were amplified in One Shot TOP10 Chemically Competent *E. coli*, miniprep purified, sequenced and transformed into One Shot BL21-AI *E. coli* strain. His-rtsAC$_T$ protein production was induced with 0.2% L-arabinose for 3 h at approximately 30°C (electronic supplementary material, figure S4). Cells were harvested by centrifugation and the pellet was stored at −80°C. After thawing, pellets were resuspended in lysis buffer (10 mM imidazole; 1 mg ml^{-1} lysozyme (Amresco), 1 : 800 benzonase nuclease (Novagen), 1 mM PMSF, 1 mM Na_3VO_4, 1 mM NaF and protease inhibitor cocktail (SIGMA); in PBS, pH 7.4). After sonication (five cycles of 10 s each on ice), lysates were incubated at room temperature on a horizontal shaker, centrifuged (21 000*g*, 30 min, 4°C). The supernatant was passed through a HisPur™ Ni-NTA resin (Thermo Fisher Scientific). His-rtsAC$_T$ was eluted with 5 ml PBS with 250 mM imidazole; pH 7.4.

2.4. Characterization of rtsAC activity

Purified recombinant rtsAC$_T$ protein (approx. 0.2 µg µl^{-1}) was incubated in triplicate with assay buffer (100 mM Tris pH 7.4, 1 mM DTT, 150 mM NaCl, 250 µM IBMX, 2.5 mM ATP, and either 5 mM $MnCl_2$ or 15 mM $MgCl_2$ + 1 mM $CaCl_2$, as indicated below). The drugs KH7, LRE1, forskolin or 2,2-DDA were dissolved in DMSO (final concentration of 0.02% v/v) and their IC_{50} values were calculated in assay buffer containing 5 mM $MnCl_2$, and controls were run with DMSO alone. The EC_{50} for HCO_3^- was measured in assay buffer containing 15 mM $MgCl_2$ and 1 mM $CaCl_2$. Finally, the effects of KH7, LRE1 and 4,4′-diisothiocyano-2,2′-stilbenedisulfonic acid (DIDS) were measured in the presence of 20 mM $NaHCO_3$ in assay buffer containing 15 mM $MgCl_2$ and 1 mM $CaCl_2$, to determine their effects on rtsAC baseline activity and on the HCO_3^--stimulated portion. These conditions were selected based on extensive optimization efforts that revealed that Mg^{2+} and Ca^{2+} were essential for sustaining HCO_3^--stimulated rtsAC activity, but did not induce a clear dose–response on sAC activity by themselves under our assay conditions.

Reactions were run for 1 h at room temperature and were stopped by addition of an equal volume of 0.2 N HCl and cAMP was quantified using the Direct cyclic AMP ELISA kit (Arbor Assays, Ann Harbor, MI, USA). Each treatment was performed using His-rtsAC$_T$ from two to five different protein purifications.

Data were analysed and plotted using GraphPad Prism 7 (La Jolla, California, USA). The EC_{50} for HCO_3^- was determined using a variable slope four parameters curve fit of log ([HCO_3^-]) versus [cAMP]. The IC_{50} values for KH7 and LRE1 were determined using a variable slope four- or three-parameter curve fit of log [KH7] or [LRE1] versus [cAMP]. Sensitivity of control and 20 mM HCO_3^--stimulated rtsAC to KH7, LRE1 and DIDS was analysed by two-way ANOVA followed by Tukey's multiple comparisons test. Statistical significance was set at $p < 0.05$. Data are presented as mean ± standard error of the mean (s.e.m.).

2.5. Cell culture

An immortalized cell line derived from rainbow trout gill, RTgill-W1 cell line (ATCC CRL-2523) [34] was cultured in modified Leibovitz's L-15 medium containing 2.05 mM L-glutamine (Hyclone, Logan, UT, USA), 10% v/v fetal bovine serum (Thermo Fisher Scientific) and 1% v/v penicillin/streptomycin solution (Thermo Fisher Scientific), and maintained at 18°C.

2.6. Western blotting and immunofluorescence

The following stocks of commercially available antibodies were used: mouse anti-Na^+/K^+-ATPase (NKA) [35], mouse anti-actin and mouse anti-α-tubulin (12G10) (all from Developmental Studies Hybridoma Bank, The University of Iowa, IA, USA), mouse anti-sarcomeric α-actinin (EA-53) (abcam, Cambridge, MA, USA), mouse anti-Golgi matrix protein of 130 kDa (GM-130) (BD Biosciences) (2.5 µg ml^{-1}); anti-rabbit and anti-mouse Alexa 555 and Alexa 488 (Invitrogen). In addition, we generated custom-made rabbit polyclonal antibodies against the peptide LSSKKGYGADELTRC in the C1 catalytic domain (anti-rtsAC-C1, 3 µg ml^{-1} stock) and against the peptide SVEREEGYPLLGREC at the beginning of the P-loop motif (anti-rtsAC-FL, 1.2 µg ml^{-1} stock) (GeneScript USA, Inc). Validation of anti-rtsAC-C1 antibodies by Western blotting using His-rtsAC$_T$ as the positive control and peptide-preabsorption controls for the various tissues is shown in electronic supplementary material, figure S4.

For Western blots, tissues were processed as previously described [20,26,36], and RTgill-W1 cells were lysed in RIPA buffer containing protease inhibitors and centrifuged (30 min, 23 000*g*, 4°C) [36]. Anti-rtsAC-C1 antibodies were applied at 1 : 5000 dilution. For immunohistochemistry, tissue samples were processed as described in [26]; staining of cardiomyocytes, white muscle, red blood cells (RBCs) and RTgill-W1 cells required optimization (detailed in electronic supplementary material).

3. Results and discussion

3.1. sAC genes are present throughout fish lineages

BLAST searches on nucleotide database confirmed the presence of sAC genes in species from all major animal phyla, including cartilaginous (Chondrichthyes), ray-finned (Actinopterygii) and lobe-finned (Sarcopterygii) fishes (electronic supplementary material, figure S1). Within the ray-finned fishes, sAC-like genes were identified in species from the subclasses Chondrostei (i.e. sturgeon) and Neopterigii (i.e. Holostei (gar) and Teleostei (teleosts)). Within the teleosts, complete or partial sAC genes were found in many species from the superorders Protacanthopterygii, Ostariophysi, Clupeomorpha and Stenopterygii (electronic supplementary material, table S2). However, we failed to obtain definitive evidence for the presence of sAC genes in Cypriniformes (a large order within the Ostariophysi that includes zebrafish), or in any Neoteleostei. These results are puzzling when considering that sAC activity seems essential for proper sperm function across a broad range of phyla, including sea urchin [37], ascidian [35], salmon [30] and human [17], which may be expected to exert a strong positive selective pressure for the retention of functional sAC genes. Interestingly, biochemical and functional evidence suggests sAC may be present in three Neoteleostei species: toadfish [29], sea bream [32] and mackerel [31], which belong to three different orders within the superorder Acanthopterygii (Batrachoidiformes, Percifomes and Scombriformes, respectively). However, a definite confirmation will await detailed studies in more fish species. Evidence for alternative splicing of sAC mRNA was found in salmonids, northern pike, ayu, channel and shark catfishes, piranha, herring and allis shad (electronic supplementary material, table S2). However, automated computational analyses align mRNA fragments with annotated gene extrons and generate the longest possible mRNA sequence, and do not necessarily reflect real mRNA splice variants. Thus, alternative splicing in trout sAC (rtsAC) was further investigated using traditional RT-PCR.

3.2. rtsAC splice variants

Due to their importance for sperm function, testis typically express a high level and heterogeneity of sAC mRNAs

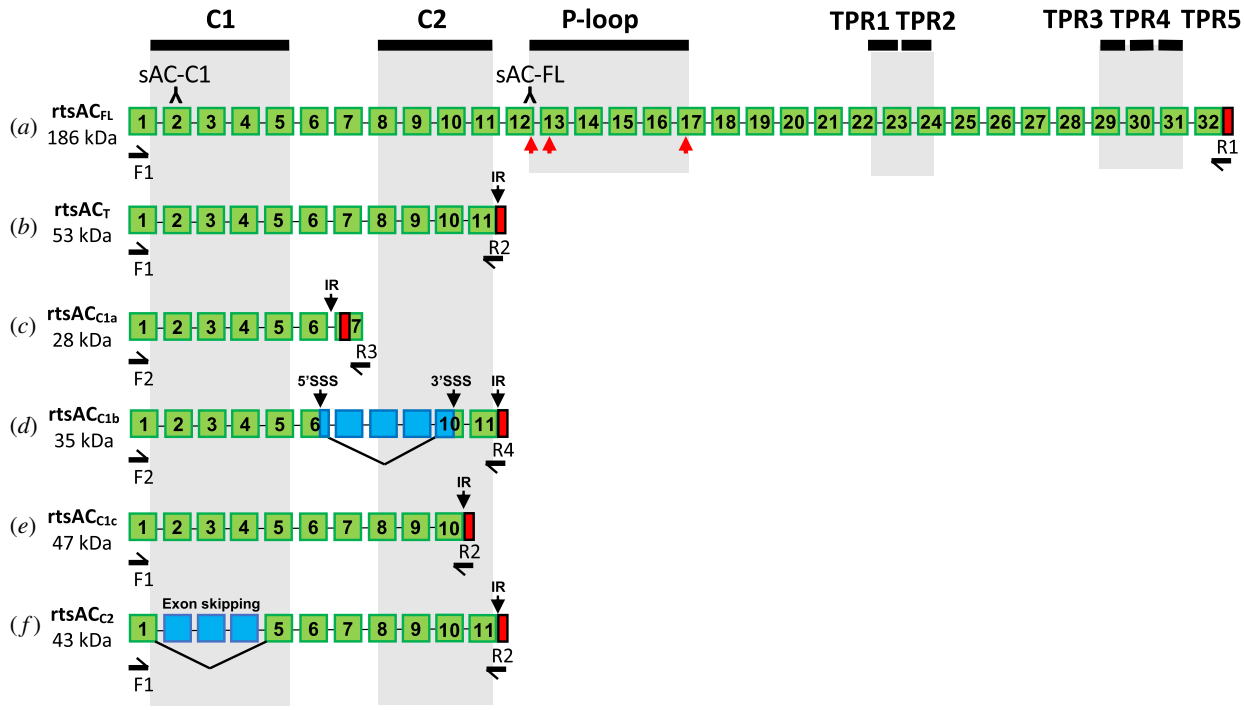

Figure 1. Schematic organization of rtsAC isoforms with complete Open Reading Frames cloned. Sequences (*a–f*) with GenBank accession nos. MF034909, MF034901, MF034907, MF034906, MF034908 and MF034905, respectively. C1 and C2: catalytic domains; green boxes: exons; red boxes: contain stop codons; blue boxes: skipped exons; inverted (Y): epitopes recognized by anti-sAC-C1 and anti-sAC-FL antibodies; P-loop: P-loop domain; TPR: tetratricopeptide repeat (TPR)-like domain (1 to 5); the red arrows in (*a*) indicate Golgi apparatus targeting sequences. IR: intron retention. 3′ and 5′SSS: alternative 3′ or 5′ splice site selection. The black arrows indicate the primer sets used to clone each sequence (F, forward; R, reverse) and are listed in table S1 (electronic supplementary material).

[6,38] and thus we chose this organ as the mRNA source for our cloning efforts. We were able to clone the complete open reading frame (ORF) of six rtsAC mRNA splice variants (figure 1) (from the eukaryotic Kozak consensus translation initiation sequence to the stop codon). The rtsAC splice variants are the result of different splicing mechanisms including exon skipping, alternative 3′ splice site selection (3′ SSS), alternative 5′ splice site selection (5′ SSS), intron retention and combinations thereof. We named the six rtsAC splice variants with complete ORF as full-length rtsAC (rtsAC$_{FL}$), truncated rtsAC (rtsAC$_{T}$), C1-only rtsACs a, b and c (rtsAC$_{C1a–c}$) and C2-only rtsAC (rtsAC$_{C2}$).

rtsAC$_{FL}$ is the longest splice variant, with an ORF of 4953 bp coding a 1650 amino acid protein with a predicted molecular weight (MW) of 186 kDa (figure 1*a*; electronic supplementary material, figure S2). The N-terminus contains the two catalytic domains C1 and C2 that are essential for cAMP production and HCO_3^- stimulation, followed by a STAND nucleotide-binding P-loop motif that also contains three Golgi apparatus targeting sequences. In the most C-terminal region, rtsAC$_{FL}$ contains five TPR motifs predicted to mediate protein–protein interactions and the assembly of multiprotein complexes [6,10,37]. For example, sAC in sea urchin sperm was reported to co-immunoprecipitate with at least 10 other proteins including a Na^+/H^+ exchanger, a cyclic nucleotide-gated channel, dynein tubulins, creatine kinase, a guanylyl cyclase and a GMP-specific phosphodiesterase [39]. In the C-terminus region, rtsAC$_{FL}$ also shows similarity to a novel haem-binding domain identified in mammalian sAC$_{FL}$, which could confer activation by NO and CO gases [40].

rtsAC$_{T}$ has a 1431 bp ORF that codes for a 476 amino acid and approximately 53 kDa protein, which contains C1 and C2 but none of the C-terminus motifs present in rtsAC$_{FL}$ (figure 1*b*). This rtsAC isoform resembles the mammalian 'truncated sAC' (sAC$_{T}$) [6]; however, while mammalian sAC$_{T}$ results from the skipping of exon 11 [24], rtsAC$_{T}$ originates from the retention of the intron after exon 11 that introduces a premature stop codon.

rtsAC$_{C1a–c}$ code for proteins containing the entire C1 but with partial or absent C2. They result from a combination of splicing mechanisms that introduce stop codons before the P-loop and TPR motifs and the Golgi targeting sequences. rtsAC$_{C1a}$ codes for a 28 kDa protein that contains exons 1–6, but contains an intron retention before exon 7 that changes the reading frame and introduces a stop codon early in exon 7. This sequence lacks part of the C1–C2 linker and the entire C2 (figure 1*c*). rtsAC$_{C1b}$ codes for a 35 kDa protein and originates by alternative 5′ SSS at exon 6, skipping of exons 7, 8 and 9 (which code for the C1–C2 linker and part of C2), 3′ SSS of exon 10, and intron retention after exon 11 introducing a stop codon (figure 1*d*). The third C1-only rtsAC variant is rtsAC$_{C1c}$, which codes for a 47 kDa protein that is the result of intron retention after exon 10 that introduces a stop codon (figure 1*e*). Compared to rtsAC$_{T}$, it lacks exon 11, which is the most C-terminal exon of C2 and contains the residues that bind ATP.

rtsAC$_{C2}$ has a 1143 bp ORF and codes for a 43 kDa protein. It skips exons 2–4, which contain residues in C1 essential for binding of catalytic cations, as well as ATP, and HCO_3^-. It contains exons 5–11, which code for the entire C2 but retains the intron after exon 11, which introduces an early stop codon. In summary, rtsAC$_{C2}$ contains C2 but lacks most of C1 (figure 1*f*).

3.3. Potential significance of C1- and C2-only rtsACs

All metazoan Class III ACs (i.e. sAC and tmACs) characterized to date contain two types of catalytic domains, C1 and

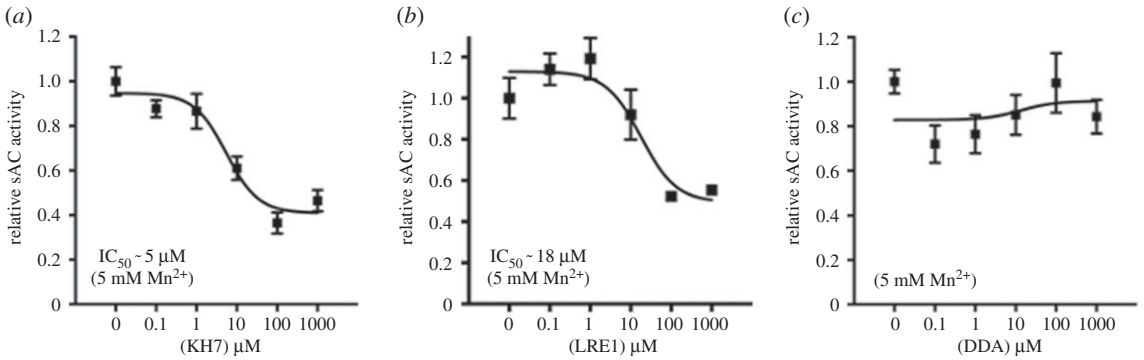

Figure 2. Effect of various inhibitors on recombinant His-rtsAC$_T$ protein. cAMP production in the presence of 5 mM Mn^{2+}, the sAC inhibitors (*a*) KH7 or (*b*) LRE1, or (*c*) the transmembrane adenylyl cyclase inhibitor 2,2-DDA. The data are shown as mean ± s.e.m. and are representative of two to four different protein purifications, each run in two to four replicates. Values are expressed as fold-stimulation relative to baseline. IC_{50}: half maximal inhibitory concentration.

C2, which are sequentially arranged within a single protein chain. C1 and C2 form an internal pseudoheterodimer with one catalytic pocket that coordinates the binding of ATP and catalytic metals enable the cyclization of ATP into cAMP [41]. By contrast, bacterial and protozoan Class III ACs typically have a single type of catalytic domain, and cAMP-forming catalytic activity depends on the formation of a homodimer between catalytic domains from two distinct protein chains [41]. While C2-only sAC isoforms are expressed in mammals [21,22], C2 homodimers do not possess the required complementary set of key amino acid residues [41] and thus do not possess cAMP-producing activity [21,23]. However, experiments on airway epithelial cells from C2 knock-out mice suggested that a C2-only sAC isoform could heterodimerize with yet-unidentified C1-only sAC isoforms and sustain cAMP production [21]. Our findings in rainbow trout provide the first evidence that C1-only sAC isoforms indeed exist, and we are currently investigating whether they can sustain functional AC activity as homodimers, or combine with C2-only sAC isoforms to form functional heterodimers.

3.4. Multiple other rtsAC splice variants

We identified 14 additional potential rtsAC splice variants comprising different combinations of exons and introns that result from a variety of splicing mechanisms (electronic supplementary material, figure S3). Unfortunately, we were unable to clone their cDNAs as single amplicons due to limitations in primer design and primer binding to multiple rtsAC cDNA sequences (see [15] for a detailed explanation). Importantly, all of the RT-PCR products were sequenced, follow established splicing mechanisms, are missing complete exons while maintaining an ORF, and/or include intronic regions. In combination, these factors strongly suggest that the cDNAs with atrial ORFs are *bona fide* rtsAC splice variants and not the result from PCR artefacts.

Sequence analyses indicate that these putative rtsAC variants are different from rtsAC$_{FL}$, rtsAC$_T$, rtsAC$_{C1a–c}$ and rtsAC$_{C2}$. Three of these splice variants were deduced from overlapping RT-PCRs, and putatively code for additional C1- or C2-only rtsACs (electronic supplementary material, figure S3G-I). Some of the other potential rtsAC splice variants would completely or partially lack a variable number of exons and could code for rtsAC isoforms of diverse sizes (electronic supplementary material, figure S3 J-T); however, large portions of their N- or C-terminus remain unknown which precluded us from definitely assessing their sizes. Interestingly, many of these putative rtsAC isoforms would lack some or all of the P-loop or TPR domains, suggesting different regulatory properties and protein–protein interactions compared to rtsAC$_{FL}$.

Overall, our results indicate the existence of extensive alternative splicing, potentially resulting in as many as 20 rtsAC isoforms. These results are consistent with multiple previous reports from a variety of other tissues and organisms and may be related to the differential subcellular localization of sAC and their association with other proteins [10,21–23,26,42–44].

3.5. Characterization of rtsAC activity

Enzymatic cAMP-producing activity was characterized using His-rtsAC$_T$. Truncated sAC proteins are ideal for this type of analyses because they generally are the most active sAC isoforms [1,6,11,17] and this facilitates more accurate cAMP measurements. In addition, they allow the characterization of catalytic activity by C1 and C2 without interference from putative regulatory domains that might be present in the C-terminus region. And although different sAC isoforms might have different V_{max}, the affinity for ATP, HCO_3^- and catalytic metals is solely determined by amino acid residues in C1 and C2 [11].

Preliminary assays revealed that His-rtsAC activity was maximal at 2.5 mM ATP. This relatively low affinity for ATP is one of the characteristics that differentiates sAC from tmACs [5,6]; however, a detailed ATP dose–response for rtsAC was not performed. Production of cAMP by His-rtsAC$_T$ was increased approximately 20-fold by 5 mM Mn^{2+}, which is another hallmark of sAC activity. Mn^{2+}-stimulated rtsAC activity was sensitive to the sAC-specific small molecule inhibitors KH7 and LRE1 ($IC_{50} \sim 5$ and 18 µM, respectively), but insensitive to DDA, a specific inhibitor of tmACs (figure 2). In the presence of more physiologically relevant 15 mM Mg^{2+} and 1 mM Ca^{2+} as catalytic metals, His-rtsAC$_T$ activity was stimulated by HCO_3^- with an EC_{50} of approximately 7 mM (figure 3*a*). This value is within the normal range of [HCO_3^-] in rainbow trout plasma [45] and closely matches the approximately 5 mM reported for sAC from the dogfish shark [9], a cartilaginous fish. These kinetic characteristics make rtsAC a suitable HCO_3^- sensor under physiologically relevant acid–base conditions typically found in the internal fluids of fish, where [HCO_3^-] ranges from nearly 0 to approximately 20 mM,

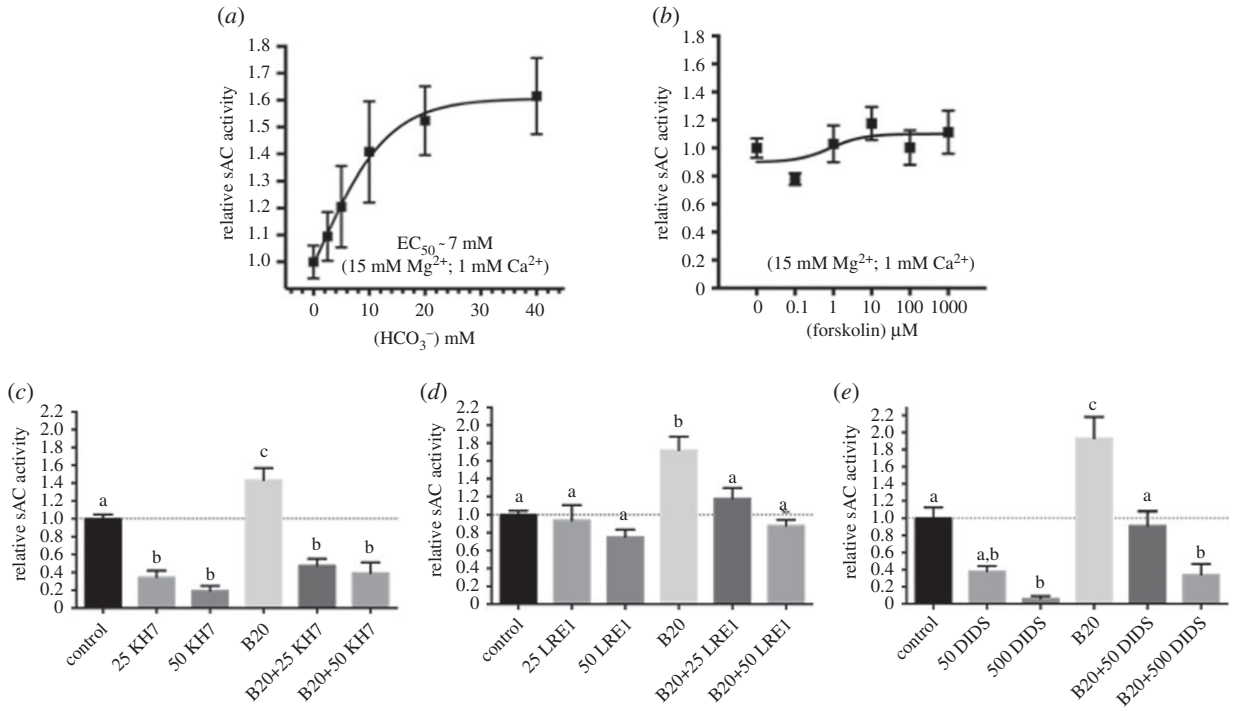

Figure 3. Biochemical characterization of recombinant His-rtsAC$_T$ protein. cAMP production in the presence of 15 mM Mg^{2+} and 1 mM Ca^{2+}: (*a*) stimulation by HCO_3^-; (*b*) effect of the transmembrane adenylyl cyclase agonist, forskolin. Effect of the sAC inhibitors (in µM) (*c*) KH7 or (*d*) LRE1, and (*e*) DIDS on His-rtsAC$_T$ activity stimulated with or without 20 mM $NaHCO_3$ (B20). Values are expressed as fold-stimulation relative to baseline. The data are shown as mean ± s.e.m. and are representative of four to five different protein purifications, each run in two to four replicates. Different letters (a, b or c) indicate $p < 0.05$. EC_{50}: half maximal effective concentration.

and pH from approximately 7.4 to approximately 8.3 [14]. In addition to Mg^{2+}, HCO_3^--stimulated rtsAC activity required 1 mM Ca^{2+} as the second catalytic metal. However, 1 mM Ca^{2+} alone did not stimulate basal rtsAC activity, nor did we find a consistent dose–response to [Ca^{2+}] under the experimental conditions used in our assays. Thus further *in vitro* and *in vivo* experiments are required to confirm whether rtsAC may also act as a Ca^{2+} and ATP sensor as reported for mammalian sAC [46–48]. Similar to mammalian sAC [6], His-rtsAC$_T$ was unaffected by the widely used tmAC stimulator, forskolin (figure 3*b*). These results validate the use of KH7, LRE1, DDA and forskolin as pharmacological agents to study cAMP signalling pathways in fish (see [15] for additional considerations).

In addition, we examined the effects of 25 and 50 µM KH7 and LRE1 on the activity of His-rtsAC$_T$ that was stimulated by 20 mM HCO_3^- (which is close to the highest physiologically relevant [HCO_3^-] in fish internal fluids [14]), in the presence of Mg^{2+} and Ca^{2+} as catalytic metals. While KH7 significantly inhibited both basal and HCO_3^--stimulated His-rtsAC$_T$ activity (figure 3*c*), LRE1 only inhibited the HCO_3^--stimulated component and had no effect on basal His-rtsAC activity (figure 3*d*). These results are consistent with more detailed pharmaco-kinetic analyses on mammalian sAC, which suggested KH7 is a mixed competitive–uncompetitive inhibitor [16,17,19], and indicated that LRE1 is a competitive inhibitor with HCO_3^- [18].

Finally, we tested the effect of DIDS on basal and HCO_3^--stimulated His-rtsAC$_T$ activity. This disulfonic stilbene compound is an inhibitor of anion exchanger proteins and is commonly used to study HCO_3^- transport processes in cells and epithelia, including many aquatic animals (e.g [49–56]). However, DIDS was recently found to also competitively inhibit mammalian sAC with [HCO_3^-]-dependent IC_{50} between approximately 40 and 130 µM [57]. Here, we demonstrate that DIDS also inhibits His-rtsAC$_T$ activity with an apparent IC_{50} of approximately 50 µM (figure 3*e*). Based on DIDS potential off-target effects on sAC-dependent signal transduction pathways, we recommend revisiting previous studies that reported effects of DIDS on HCO_3^--dependent processes and discourage its use in future studies.

3.6. rtsAC expression and localization in various rainbow trout tissues

The presence of multiple rtsAC splice variants together with a generally low mRNA abundance in tissues other than testis greatly complicated the identification of sAC splice variants using RT-PCR or other transcriptomic techniques [15]. Therefore, we probed selected rainbow trout tissues using Western blotting with anti-rtsAC-C1 antibodies, and visualized the cellular localization of rtsAC by immunohistochemistry and immunocytochemistry. Western blotting revealed protein bands of varied sizes, which demonstrated tissue-specific expression patterns. Some of the bands were consistent with the rtsAC splice variants with complete ORF shown in figure 1 (i.e. 186, 53, 47, 43, 35 and 28 kDa). Other bands hinted at the presence of rtsAC isoforms of approximately 70, 90 and 100–110 kDa that could correspond to some of the splice variants shown in electronic supplementary material, figure S3, and additionally matched the sizes of known sAC isoforms in mammals [21,23], coral [10] and sharks [9], respectively. Because the immunoreactive bands were absent in the peptide preabsorption controls (electronic

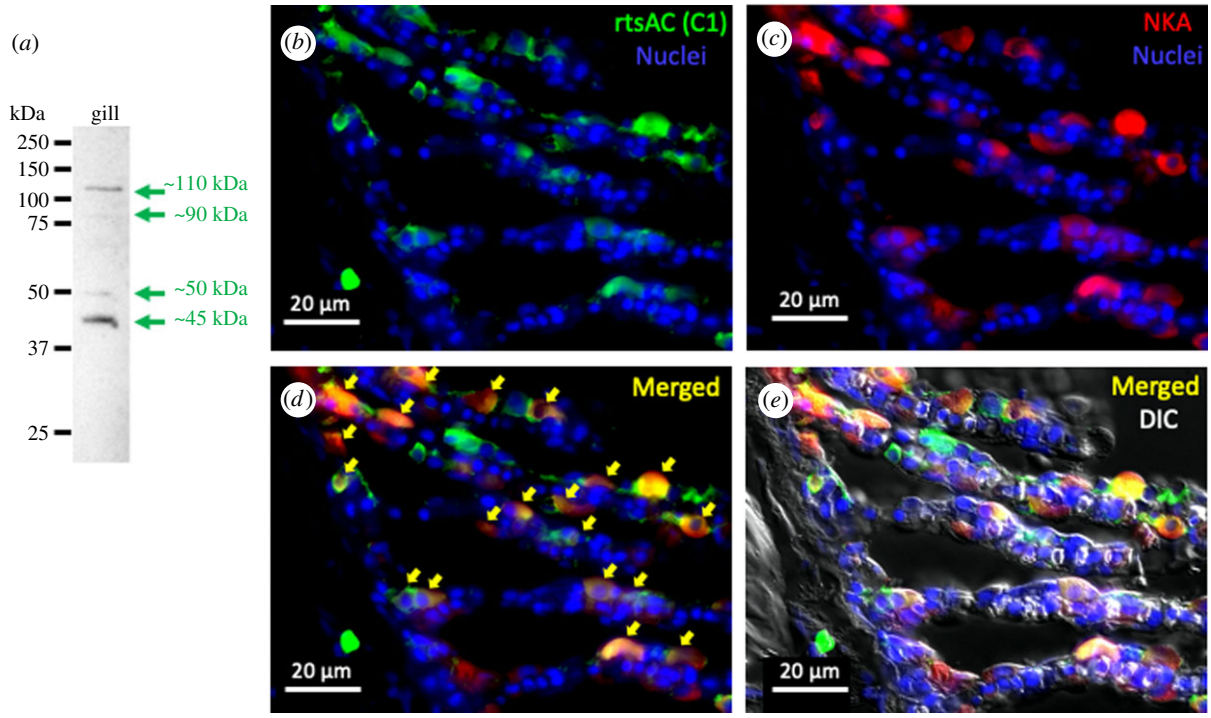

Figure 4. The presence and localization of rtsAC protein in trout gill cells. (*a*) Western blot of gill tissue probed with anti-rtsAC-C1 antibodies detected four bands ranging from approximately 45 to approximately 110 kDa. Gill filament and lamellae co-immunostained with (*b*) anti-rtsAC-C1 (green), and (*c*) Na^+-K^+-ATPase (NKA, red) antibodies. (*d*) sAC was highly expressed in NKA-rich ionocytes, which are cells specialized for acid/base and ionic regulation (arrows). Co-localization of sAC and NKA antibodies appears yellow. (*e*) Immunofluorescence image merged with differential interference contrast (DIC). Nuclei were labelled with Hoechst 33342 (blue).

supplementary material, figure S4) and the epitope recognized by the anti-rtsAC antibodies is not preset in any other protein found in trout databases, we are confident these bands represent authentic rtsAC isoforms; however, this should be confirmed in future research. Similarly establishing the functional significance of the observed tissue-differential expression of multiple rtsAC isoforms across tissues awaits future experiments to determine the roles of C1- and C2-only rtsAC isoforms, and of the different sAC domains in rtsACs or of homologous domains in sACs from other organisms.

The gills are the main acid–base regulatory organs in many aquatic organisms, and their function is in many ways analogous to that of the mammalian kidney [58]. Previous studies have established that sAC is a physiological acid–base sensor in ion-transporting cells from both elasmobranch fish gills [9,20] and the mammalian kidney [59–61]. Here, we show that rainbow trout gills may express four rtsAC isoforms of approximately 45, approximately 50, approximately 90 and approximately 110 kDa (figure 4*a*). Furthermore, rtsAC is preferentially present in Na^+/K^+-ATPase-rich gill ionocytes as well as in another epithelial cell subtype with reduced or absent Na^+/K^+-ATPase expression (figure 4*b–e*). Presumably, these are the acid- and base-secreting cells [62], suggesting rtsAC plays important roles in both processes as well as in NaCl uptake for osmoregulatory purposes (unlike the gills from marine sharks, the gills of freshwater fishes play a dual role in acid–base and osmotic regulation).

The expression of rtsAC was highest in heart and white muscle tissue. Both tissues predominantly expressed an approximately 50 kDa protein, most likely $rtsAC_T$ (figure 5*a*). However, there were some differences in the expression levels of some other rtsAC isoforms, most notably an approximate 90 kDa isoform in heart and an approximate 70 kDa isoform in white muscle. Immunocytochemistry on isolated cardiomyocytes revealed that rtsAC is present in distinct subcellular regions including the sarcomere M- and Z-lines, and potentially the sarcoplasmic reticulum (figure 5*c–f*). We have previously reported the presence of sAC in the heart of shark [26] and Pacific hagfish [63], and in the white muscle of shark [26]. In the hagfish heart, sAC activity is involved in sustaining tachycardia during recovery from anoxia [63]. In the mammalian heart, sAC was originally found to participate in the mitochondrial apoptosis pathway [64], but more recent studies have revealed that sAC_T plays additional roles in modulating cardiac contractility [65] and cardiac hypertrophy [66]. Our results suggest that sAC may play similar functions in the teleost heart; however, the lack of t-tubules in non-mammalian vertebrates [67] is likely associated with species-specific sAC-dependent regulation that will be determined through future research. In white muscle (figure 5*b*), rtsAC exhibits a similar localization pattern compared to that in cardiomyocytes. The lack of previous studies on sAC in mammalian white muscle prevents us from proposing potential roles. However, white muscle is by far the most abundant fibre type in fish and relies heavily on glycolytic ATP production to power rapid muscle contraction. Whether sAC activity plays a functional role in fish locomotion and whether this putative modulation is in response to HCO_3^-, Ca^{2+} and/or ATP remains to be studied.

In the rainbow trout liver, the most abundant rtsAC isoforms were approximately 50 kDa (consistent with $rtsAC_T$) and approximately 70 kDa (electronic supplementary material, figure S5A). The localization of rtsAC was fairly homogeneous throughout the hepatocyte cytoplasm, with some hints of nuclear localization in a minority of cells (electronic supplementary material, figure S5B,C). Based on reports from mammalian liver cells, potential functions

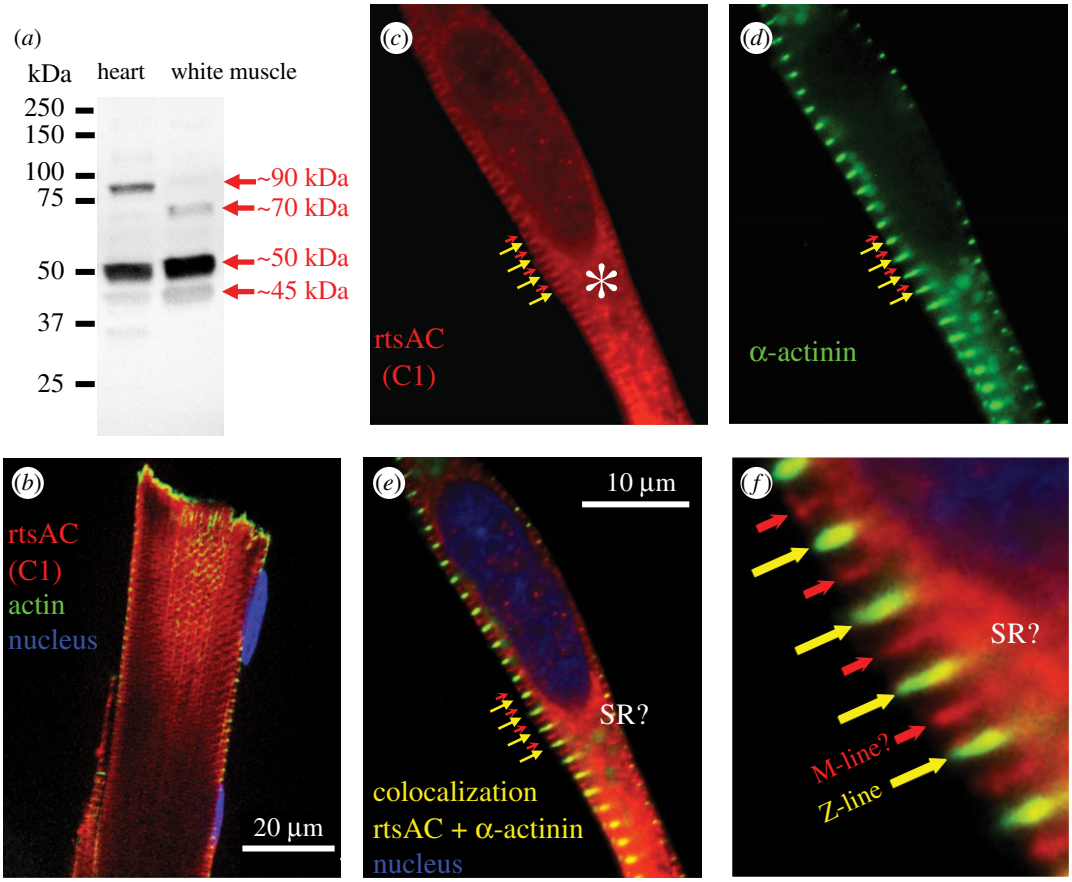

Figure 5. The presence and localization of rtsAC protein in trout striated muscle. (*a*) Western blot of heart and white muscle tissue probed with anti-rtsAC-C1 antibodies detected different bands ranging from approximately 45 to approximately 90 kDa. (*b*) Isolated white muscle fibres co-immunostained with anti-rtsAC-C1 (red) and anti-actin (green) antibodies. (*c–f*) Isolated cardiomyocytes were co-immunostained with anti-rtsAC-C1 (red) and anti-α-actinin (green) antibodies, the latter labels sarcomeric Z-lines. The merged images (*e*,*f*) show sAC presence in Z-lines (yellow arrows, *f*), in a region consistent with M-lines (red arrows, *f*), and in a region consistent with the sarcoplasmic reticulum (SR, asterisk, *c*). Nuclei were labelled with Hoechst 33342 (blue).

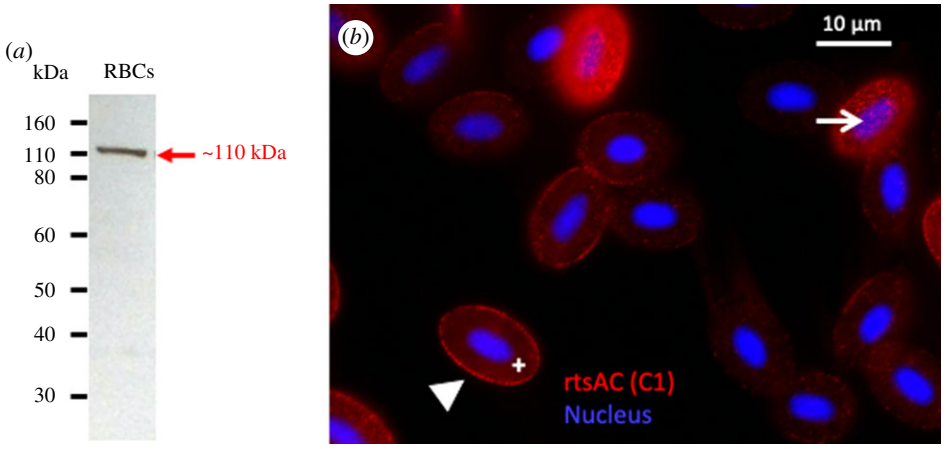

Figure 6. The presence and localization of rtsAC protein in trout RBCs. (*a*) Western blot of rainbow trout RBCs probed with anti-rtsAC-C1 antibodies detected a band at approximately 110 kDa. (*b*) RBCs immunostained with anti-rtsAC-C1 antibodies (red) showed the presence of sAC in the cytoplasm (+), plasma membrane (arrow head) and nucleus (arrow). Nuclei were labelled with Hoechst 33342 (blue).

in fish liver may include the regulations of the transcription factor CREB [68] and of Cl^- and HCO_3^- driven cholangiocyte fluid secretion [69]. Western blotting additionally revealed rtsAC presence in the trout intestine and inner ear (electronic supplementary material, figure S4).

We also found robust expression of rtsAC within RBCs, which seemed to exclusively express an approximately 110 kDa rtsAC isoform (figure 6*a*). Immunocytochemical analyses revealed rtsAC is present throughout the RBC cytoplasm, but also in association with the plasma membrane and both around and within the nucleus (figure 6*b*). To our knowledge, the only previous report of sAC in RBCs was in shark [2], where a protein of similar size is recognized by specific anti-shark sAC antibodies. However, evidence for any functional roles of sAC in RBCs is lacking. Given the cyclical fluctuations in acid–base conditions experienced by

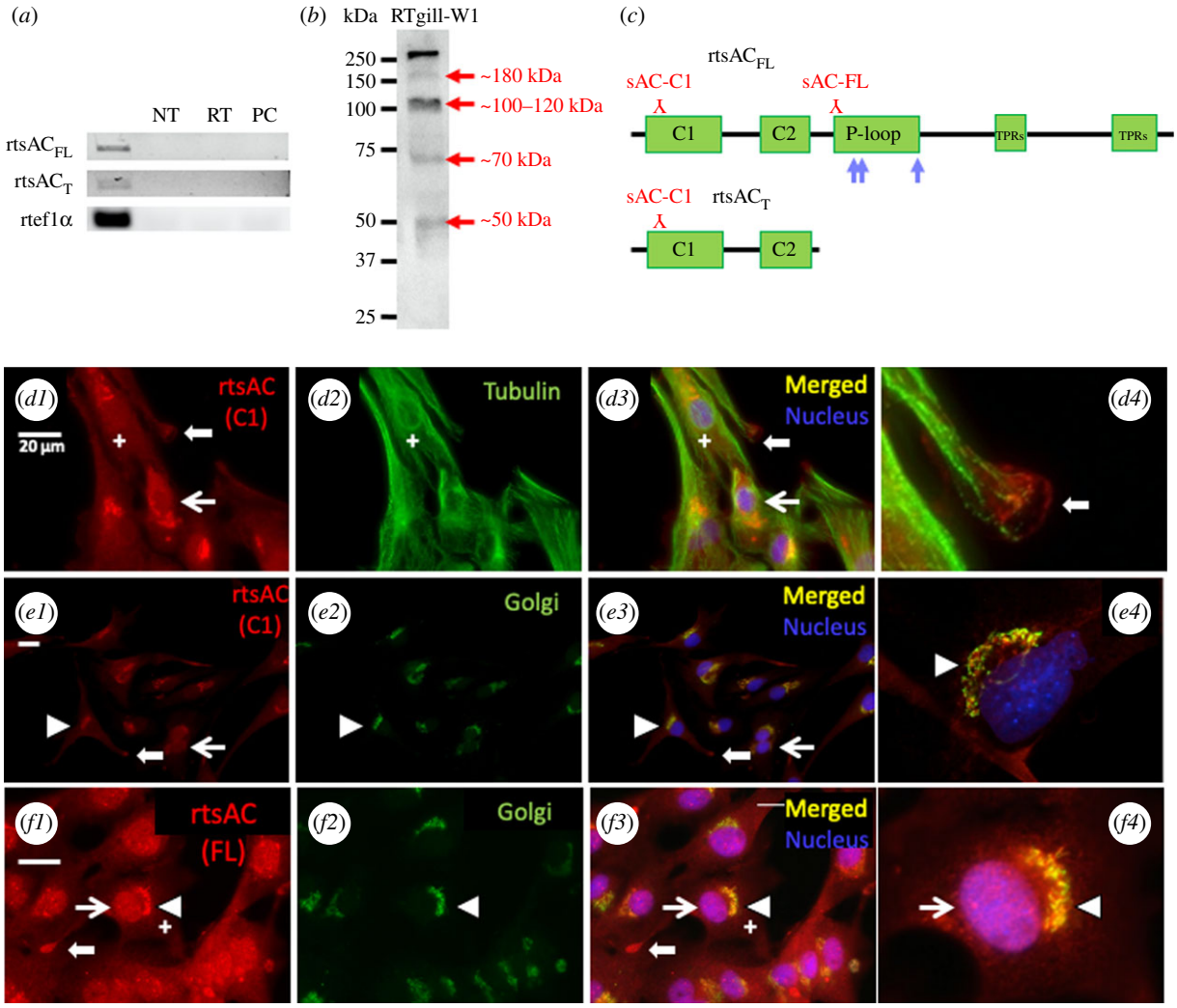

Figure 7. The presence and localization of rtsAC protein in RTgill-W1 cells. (*a*) RT-PCR detected the two rtsAC splice variants, full-length ($rtsAC_{FL}$) and truncated ($rtsAC_T$). Elongation factor 1 alpha (ef1α) served as internal control. NT, no template control; RT, no reverse transcriptase control; PC, PCR control. (*b*) Western blot of RTgill-W1 cells using anti-rtsAC-C1 antibodies detected bands ranging from approximately 50 to greater than 250 kDa. (*c*) Schematic of the $rtsAC_{FL}$ and $rtsAC_T$ proteins; C1 and C2: catalytic domains. P-loop: P-loop domain. TPRs: tetratricopeptide repeat (TPR)-like domains. Inverted (Y): epitopes recognized by anti-sAC-C1 and anti-sAC-FL antibodies. Arrows: Golgi apparatus targeting sequences. Immunostaining of RTgill-W1 cells using anti-rtsAC-C1 antibodies (red) (panels *d*1, *d*3, *d*4 and *e*1, *e*3, *e*4) with alpha-tubulin (Tubulin, green) (panels *d*2–*d*4) or with Golgi apparatus marker (Golgi matrix protein of 130 kDa or GM130, green; panels *e*2–*e*4); or anti-rtsAC-FL (red; panels *f*1, *f*3, *f*4) with GM-130 (panels *f*2–*f*4). Nuclei were labelled with Hoechst 33342 (blue). Co-localization is seen as yellow (Merged). Arrowheads indicate Golgi apparatus, wide arrows podosome-like structures, thin arrows nuclei and (+) cytoplasm. Scale bars = 20 µm.

RBCs with every pass through the circulatory system and the role of intracellular pH in modulating haemoglobin O_2 and CO_2 binding (reviewed in [70]), sAC may play important roles in RBC physiology and whole-animal gas exchange.

3.7. Subcellular localization of rtsAC isoforms in RTgill-W1 cells

Finally, we studied the subcellular localization of rtsAC isoforms in more detail in RTgill-W1 cells, an immortalized cell line derived from rainbow trout gills [34]. These cells are widely used for *in vitro* studies in fish toxicology, virology and biochemistry [71–73] and their large size and flat morphology facilitate microscopy studies. RT-PCR detected mRNA for $rtsAC_{FL}$ and $rtsAC_T$ (figure 7*a*) as well as several additional amplicons indicating multiple other rtsAC splice variants. Western blots with anti-rtsAC-C1 antibodies (figure 7*b*) revealed protein bands consistent with $rtsAC_{FL}$ (approx. 180 kDa) and $rtsAC_T$ (approx. 50 kDa) as well as approximately 100 and approximately 70 kDa bands that resemble those seen in gills and white muscle, respectively. Additionally, there was a protein band of very high MW (greater than 250 kDa), which might have resulted from SDS-resistant complexes between rtsAC with other proteins, or from protein aggregation artefacts.

Immunocytochemistry on RTgill-W1 cells using anti-rtsAC-C1 antibodies detected rtsAC presence in various intracellular compartments including the cytoplasm, podosome-like structures, the nucleus and the Golgi apparatus (figure 7*d*,*e*). Based on a lack of co-localization with mitotracker (electronic supplementary material, figure S6), rtsAC isoforms with the C1 motif do not appear to be present in RTgill-W1 mitochondria; however, this may be re-evaluated after optimization of alternative fixation protocols. In an attempt to study differential subcellular localization of rtsAC isoforms, we generated other custom-made polyclonal antibodies, these ones against a peptide located in the beginning of the P-loop (anti-rtsAC-FL; figure 7*c*). Unfortunately, these antibodies did not work for Western blotting; however, they intensely stained the nucleus, the Golgi apparatus and

podosomes of RTgill-W1 cells (figure 7*f*). These results suggest that longer rtsAC isoforms are preferentially expressed in these compartments; however, the epitope that is recognized by the anti-rtsAC-FL antibodies is present in at least nine of the cloned rtsAC isoforms (electronic supplementary material, figure S3), precluding further speculation. Nonetheless, it is worth mentioning that not all those rtsAC variants possess the three Golgi apparatus targeting sequences, which further narrows down the options for rtsAC isoforms that might be present in that compartment.

Research on mammals has reported sAC localization in the nucleus of hepatocytes, COS-7, Huh7 and HeLa cells [68,74], and in the peri-nuclear region (described as 'discrete dotlike Golgi staining') of some benign melanomas [75] and some virally infected keratinocytes [76]. However, to our knowledge this is the first conclusive report about the association of sAC with the Golgi apparatus, based on co-localization with the specific marker GM-130 (figure 7*e,f*). Similarly, while sAC-dependent cAMP signalling was deemed important for leucocyte transendothelial migration [77] and for neutrophil TNF activation [48], the experiments described here are the first to visualize the presence of sAC in podosome-like structures.

4. Conclusion

This study definitely establishes that sAC is present and functional in a subset of ray-finned fishes, and we hope that the molecular and biochemical characterization of rtsAC presented herein will help advance our knowledge about the roles of sAC in rainbow trout and other ray-finned fishes. The ability of sAC to respond to changes in intracellular HCO_3^- concentration and its downstream cAMP signalling pathway may allow sAC to function as a general sensor of intracellular acid–base status across a variety of different tissues in rainbow trout. In addition, we report novel observations on the presence and localization of sAC in gills from freshwater fish, in myocytes, and in RBCs. Whether sAC plays a role in modulating transepithelial NaCl uptake for hyperosmoregulation, muscle contraction during a fatigue-induced acidosis or pH-sensitive oxygen transport within RBCs remains to be investigated. Ultimately, the roles of sAC will depend on the sAC variants that are expressed within each cell type and on their functional association with upstream proteins that may affect sAC stimulation (i.e. CAs, HCO_3^- transporters and CO_2 channels), other components of the cAMP pathway (i.e. PKA, EPAC, cyclic nucleotide-gated channels), and downstream effector proteins. In addition, some of these putative novel functions, as well as those played by sAC in podosomes and the Golgi apparatus, may also apply to mammals and may guide future biomedical research.

Ethics. Procedures involving fish were approved by animal care protocols from the University of Alberta (AUP00001126 and AUP00000072), University of Exeter (PPL P88687E07) and University of Manchester (HO lic 40/3584).

Data accessibility. All data are available in the paper and electronic supplementary material.

Authors' contributions. M.T. conceived the project. C.S. performed all the molecular and cell culture work, and some of the other experiments. M.T., T.S.H., J.N.R. and G.T.K. performed some of the Western blots and immunolocalization experiments. S.D.B., G.G.G., H.S. and R.W. provided the trout tissue samples. J.L.R., H.A.S., G.G.G. and R.W.W. provided advice on potential roles of sAC in different trout cell types. M.T. and C.S. analysed the results and wrote the paper. All authors edited the manuscript and approved the final version.

Competing interests. The authors declare no competing interests.

Funding. This work was supported by grants from the National Science Foundation (USA) to M.T. (NSF IOS 1354181 and 1754994) and from the Biotechnology and Biological Sciences Research Council (UK) to R.W.W. (BBSRC BB/N013344/1), a UCSD Chancellor's Research Excellence Scholarship (CRES) to M.T. and C.S., a Company of Biologists Travel grant to C.S. (JEBTF-161115).

Acknowledgements. We are grateful to Dr Niels Bols and Dr Nathan Vo from the University of Waterloo (Canada) for providing the RTgill-W1 cell line. Angus Thies provided useful advice for the phylogenetic analysis. We also thank Dr Sébastien Santini (CNRS/Aix-Marseilles Université) for maintaining the Phylogeny.fr website.

References

1. Chen Y, Cann MJ, Litvin TN, Iourgenko V, Sinclair ML, Levin LR, Buck J. 2000 Soluble adenylyl cyclase as an evolutionarily conserved bicarbonate sensor. *Science* **289**, 625–628. (doi:10.1126/science.289.5479.625)
2. Tresguerres M, Barott KL, Barron ME, Roa JN. 2014 Established and potential physiological roles of bicarbonate-sensing soluble adenylyl cyclase (sAC) in aquatic animals. *J. Exp. Biol.* **217**, 663–672. (doi:10.1242/jeb.086157)
3. Tresguerres M, Levin LR, Buck J. 2011 Intracellular cAMP signaling by soluble adenylyl cyclase. *Kidne Int.* **79**, 1277–1288. (doi:10.1038/ki.2011.95)
4. Braun T, Dods RF. 1975 Development of a Mn^{2+}-sensitive, 'soluble' adenylate cyclase in rat testis. *Proc. Natl Acad. Sci. USA* **72**, 1097–1101. (doi:10.1073/pnas.72.3.1097)
5. Braun T. 1991 Purification of soluble form of adenylyl cyclase from testes. *Methods Enzymol.* **195**, 130–136. (doi:10.1016/0076-6879(91)95160-L)
6. Buck J, Sinclair ML, Schapal L, Cann MJ, Levin LR. 1999 Cytosolic adenylyl cyclase defines a unique signaling molecule in mammals. *Proc. Natl Acad. Sci. USA* **96**, 79–84. (doi:10.1073/pnas.96.1.79)
7. Roelofs J, Van Haastert PJM. 2002 Deducing the origin of soluble adenylyl cyclase, a gene lost in multiple lineages. *Mol. Biol. Evol.* **19**, 2239–2246. (doi:10.1093/oxfordjournals.molbev.a004047)
8. Nomura M, Beltrán C, Darszon A, Vacquier VD. 2005 A soluble adenylyl cyclase from sea urchin spermatozoa. *Gene* **353**, 231–238. (doi:10.1016/j.gene.2005.04.034)
9. Tresguerres M, Parks SK, Salazar E, Levin LR, Goss GG, Buck J. 2010 Bicarbonate-sensing soluble adenylyl cyclase is an essential sensor for acid/base homeostasis. *Proc. Natl Acad. Sci. USA* **107**, 442–447. (doi:10.1073/pnas.0911790107)
10. Barott KL, Barron ME, Tresguerres M. 2017 Identification of a molecular pH sensor in coral. *Proc. R. Soc. B* **284**, 20171769. (doi:10.1098/rspb.2017.1769)
11. Chaloupka JA, Bullock SA, Iourgenko V, Levin LR, Buck J. 2006 Autoinhibitory regulation of soluble adenylyl cyclase. *Mol. Reprod. Dev.* **73**, 361–368. (doi:10.1002/mrd.20409)
12. Litvin TN, Kamenetsky M, Zarifyan A, Buck J, Levin LR. 2003 Kinetic properties of 'soluble' adenylyl cyclase. Synergism between calcium and bicarbonate. *J. Biol. Chem.* **278**, 15 922–15 926. (doi:10.1074/jbc.M212475200)
13. Buck J, Levin LR. 2014 The role of soluble adenylyl cyclase in health and disease. *Biochim. Biophys. Acta.* **1842**, 2533–2534. (doi:10.1016/j.bbadis.2014.09.009)

14. Tresguerres M. 2014 sAC from aquatic organisms as a model to study the evolution of acid/base sensing. *Biochim. Biophys. Acta* **1842**, 2629–2635. (doi:10.1016/j.bbadis.2014.06.021)
15. Tresguerres M, Salmerón C. 2018 Molecular, enzymatic, and cellular characterization of soluble adenylyl cyclase from aquatic animals. *Methods Enzymol.* **605**, 525–549. (doi:10.1016/bs.mie.2018.02.022)
16. Bitterman JL, Ramos-Espiritu L, Diaz A, Levin LR, Buck J. 2013 Pharmacological distinction between soluble and transmembrane adenylyl cyclases. *J. Pharmacol. Exp. Ther.* **347**, 589–598. (doi:10.1124/jpet.113.208496)
17. Hess KC *et al.* 2005 The 'soluble' adenylyl cyclase in sperm mediates multiple signaling events required for fertilization. *Dev. Cell.* **9**, 249–259. (doi:10.1016/j.devcel.2005.06.007)
18. Ramos-Espiritu L *et al.* 2016 Discovery of LRE1 as a specific and allosteric inhibitor of soluble adenylyl cyclase. *Nat. Chem. Biol.* **12**, 838–844. (doi:10.1038/nchembio.2151)
19. Steegborn C. 2014 Structure, mechanism, and regulation of soluble adenylyl cyclases: similarities and differences to transmembrane adenylyl cyclases. *Biochim. Biophys. Acta* **1842**, 2535–2547. (doi:10.1016/j.bbadis.2014.08.012)
20. Roa JN, Tresguerres M. 2016 Soluble adenylyl cyclase is an acid-base sensor in epithelial base-secreting cells. *Am. J. Physiol. Cell Physiol.* **311**, C340–C349. (doi:10.1152/ajpcell.00089.2016)
21. Chen X, Baumlin N, Buck J, Levin LR, Fregien N, Salathe M. 2014 A soluble adenylyl cyclase form targets to axonemes and rescues beat regulation in soluble adenylyl cyclase knockout mice. *Am. J. Respir. Cell Mol. Biol.* **51**, 750–760. (doi:10.1165/rcmb.2013-0542OC)
22. Farrell J, Ramos L, Tresguerres M, Kamenetsky M, Levin LR, Buck J. 2008 Somatic 'soluble' adenylyl cyclase isoforms are unaffected in $Sacy^{tm1Lex\$}$/$Sacy^{tm1Lex\$}$ 'knockout' mice. *PLoS ONE* **3**, e3251. (doi:10.1371/journal.pone.0003251)
23. Geng W, Wang Z, Zhang J, Reed BY, Pak CYC, Moe OW. 2005 Cloning and characterization of the human soluble adenylyl cyclase. *AJP Cell Physiol.* **288**, C1305–C1316. (doi:10.1152/ajpcell.00584.2004)
24. Jaiswal BS, Conti M. 2001 Identification and functional analysis of splice variants of the germ cell soluble adenylyl cyclase. *J. Biol. Chem.* **276**, 31 698–31 708. (doi:10.1074/jbc.M011698200)
25. Schmid A *et al.* 2007 Soluble adenylyl cyclase is localized to cilia and contributes to ciliary beat frequency regulation via production of cAMP. *J. Gen. Physiol.* **130**, 99–109. (doi:10.1085/jgp.200709784)
26. Roa JN, Tresguerres M. 2017 Bicarbonate-sensing soluble adenylyl cyclase is present in the cell cytoplasm and nucleus of multiple shark tissues. *Physiol. Rep.* **24**, e13090. (doi:10.14814/phy2.13090)
27. Tresguerres M, Milsom WK, Perry SF. 2019 CO_2 and acid-base sensing. In *Fish physiology* (eds M Grosell, PL Munday, AP Farrell, CJ Brauner), pp. 33–68. San Diego, CA: Academic Press.
28. Heisler N. 1988 Acid-base regulation. In *Physiology of elasmobranch fishes* (ed. TJ Shuttleworth), pp. 215–252. Berlin, Germany: Springer.
29. Tresguerres M, Levin LR, Buck J, Grosell M. 2010 Modulation of NaCl absorption by [HCO_3^-] in the marine teleost intestine is mediated by soluble adenylyl cyclase. *AJP Regul. Integr. Comp. Physiol.* **299**, R62–R71. (doi:10.1152/ajpregu.00761.2009)
30. von Schalburg KR, Gowen BE, Leong JS, Rondeau EB, Davidson WS, Koop BF. 2018 Subcellular localization and characterization of estrogenic pathway regulators and mediators in Atlantic salmon spermatozoal cells. *Histochem. Cell Biol.* **149**, 75–96. (doi:10.1007/s00418-017-1611-3)
31. Kwan GF, Smith TR, Tresguerres M. 2020 Immunological characterization of two types of ionocytes in the inner ear epithelium of Pacific Chub Mackerel (*Scomber japonicus*). *J. Comp. Physiol. B* **190**, 419–431. (doi:10.1007/s00360-020-01276-3)
32. Carvalho ESM, Gregório SF, Power DM, Canário AVM, Fuentes J. 2012 Water absorption and bicarbonate secretion in the intestine of the sea bream are regulated by transmembrane and soluble adenylyl cyclase stimulation. *J. Comp. Physiol. B* **182**, 1069–1080. (doi:10.1007/s00360-012-0685-4)
33. Dereeper A *et al.* 2008 Phylogeny.fr: robust phylogenetic analysis for the non-specialist. *Nucleic Acids Res.* **36**(Web Server issue), W465–W469. (doi:10.1093/nar/gkn180)
34. Bols NC, Barlian A, Chirino-Trejo M, Caldwell SJ, Goegan P, Lee LEJ. 1994 Development of a cell line from primary cultures of rainbow trout, *Oncorhynchus mykiss* (Walbaum), gills. *J. Fish Dis.* **17**, 601–611. (doi:10.1111/j.1365-2761.1994.tb00258.x)
35. Shiba K, Inaba K. 2014 Distinct roles of soluble and transmembrane adenylyl cyclases in the regulation of flagellar motility in Ciona sperm. *Int. J. Msol. Sci.* **15**, 13 192–13 208. (doi:10.3390/ijms150813192)
36. Roa JN, Munévar CL, Tresguerres M. 2014 Feeding induces translocation of vacuolar proton ATPase and pendrin to the membrane of leopard shark (*Triakis semifasciata*) mitochondrion-rich gill cells. *Comp. Biochem. Physiol. A Mol. Integr. Physiol.* **174**, 29–37. (doi:10.1016/j.cbpa.2014.04.003)
37. Vacquier VD, Loza-Huerta A, García-Rincón J, Darszon A, Beltrán C. 2014 Soluble adenylyl cyclase of sea urchin spermatozoa. *Biochim. Biophys. Acta* **1842**, 2621–2628. (doi:10.1016/j.bbadis.2014.07.011)
38. Sinclair ML, Wang XY, Mattia M, Conti M, Buck J, Wolgemuth DJ, Levin LR. 2000 Specific expression of soluble adenylyl cyclase in male germ cells. *Mol. Reprod. Dev.* **56**, 6–11. (doi:10.1002/(SICI)1098-2795(200005)56:1<6::AID-MRD2>3.0.CO;2-M)
39. Nomura M, Vacquier VD. 2006 Proteins associated with soluble adenylyl cyclase in sea urchin sperm flagella. *Cell Motil. Cytoskeleton* **63**, 582–590. (doi:10.1002/cm.20147)
40. Middelhaufe S, Leipelt M, Levin LR, Buck J, Steegborn C. 2012 Identification of a haem domain in human soluble adenylate cyclase. *Biosci. Rep.* **32**, 491–499. (doi:10.1042/BSR20120051)
41. Linder JU, Schultz JE. 2003 The class III adenylyl cyclases: multi-purpose signalling modules. *Cell. Signal.* **15**, 1081–1089. (doi:10.1016/S0898-6568(03)00130-X)
42. Chen J, Martinez J, Milner TA, Buck J, Levin LR. 2013 Neuronal expression of soluble adenylyl cyclase in the mammalian brain. *Brain Res.* **1518**, 1–8. (doi:10.1016/j.brainres.2013.04.027)
43. Sun XC, Cui M, Bonanno JA. 2004 [HCO_3^-]-regulated expression and activity of soluble adenylyl cyclase in corneal endothelial and Calu-3 cells. *BMC Physiol.* **4**, 8. (doi:10.1186/1472-6793-4-8)
44. Geng W, Hill K, Zerwekh JE, Kohler T, Müller R, Moe OW. 2009 Inhibition of osteoclast formation and function by bicarbonate: role of soluble adenylyl cyclase. *J. Cell. Physiol.* **220**, 332–340. (doi:10.1002/jcp.21767)
45. Cameron JN, Randall DJ. 1972 The effect of increased ambient CO_2 on arterial CO_2 tension, CO_2 content and pH in rainbow trout. *J. Exp. Biol.* **57**, 673–680.
46. Ramos LS, Zippin JH, Kamenetsky M, Buck J, Levin LR. 2008 Glucose and GLP-1 stimulate cAMP production via distinct adenylyl cyclases in INS-1E insulinoma cells. *J. Gen. Physiol.* **132**, 329–338. (doi:10.1085/jgp.200810044)
47. Zippin JH *et al.* 2013 CO_2/HCO_3^-- and calcium-regulated soluble adenylyl cyclase as a physiological ATP sensor. *J. Biol. Chem.* **288**, 33 283–33 291. (doi:10.1074/jbc.M113.510073)
48. Han H *et al.* 2005 Calcium-sensing soluble adenylyl cyclase mediates TNF signal transduction in human neutrophils. *J. Exp. Med.* **202**, 353–361. (doi:10.1084/jem.20050778)
49. Parks SK, Tresguerres M, Goss GG. 2007 Interactions between Na^+ channels and Na^+-HCO_3^- cotransporters in the freshwater fish gill MR cell: a model for transepithelial Na^+ uptake. *Am. J. Physiol. Cell Physiol.* **292**, C935–C944. (doi:10.1152/ajpcell.00604.2005)
50. Hailey DW, Roberts B, Owens KN, Stewart AK, Linbo T, Pujol R, Alper SL, Rubel EW, Raible DW. 2012 Loss of Slc4a1b chloride/bicarbonate exchanger function protects mechanosensory hair cells from aminoglycoside damage in the zebrafish mutant persephone. *PLoS Genet.* **8**, e1002971. (doi:10.1371/journal.pgen.1002971)
51. Nikinmaa M, Huestis WH. 1984 Adrenergic swelling of nucleated erythrocytes: cellular mechanisms in a bird, domestic goose, and two teleosts, striped bass and rainbow trout. *J. Exp. Biol.* **113**, 215–224.
52. Tresguerres M, Parks SK, Sabatini SE, Goss GG, Luquet CM. 2008 Regulation of ion transport by pH and [HCO_3^-] in isolated gills of the crab *Neohelice (Chasmagnathus) granulata*. *AJP Regul. Integr. Comp. Physiol.* **294**, R1033–R1043. (doi:10.1152/ajpregu.00516.2007)
53. Wilson JM, Moreira-Silva J, Delgado ILS, Ebanks SC, Vijayan MM, Coimbra J, Grosell M. 2013 Mechanisms of transepithelial ammonia excretion and luminal alkalinization in the gut of an intestinal air-breathing fish, *Misgurnus anguilliacaudatus*.

J. Exp. Biol. **216**, 623–632. (doi:10.1242/jeb.074401)

54. Jagadeshwaran U, Onken H, Hardy M, Moffett SB, Moffett DF. 2010 Cellular mechanisms of acid secretion in the posterior midgut of the larval mosquito (*Aedes aegypti*). *J. Exp. Biol.* **213**, 295–300. (doi:10.1242/jeb.037549)
55. Furimsky M, Moon TW, Perry SF. 2000 Evidence for the role of a Na^+/HCO_3^- cotransporter in trout hepatocyte pHi regulation. *J. Exp. Biol.* **203**, 2201–2208.
56. Tambutté E, Allemand D, Mueller E, Jaubert J. 1996 A compartmental approach to the mechanism of calcification in hermatypic corals. *J. Exp. Biol.* **199**, 1029–1041.
57. Kleinboelting S, Diaz A, Moniot S, van den Heuvel J, Weyand M, Levin LR, Buck J, Steegborn C. 2014 Crystal structures of human soluble adenylyl cyclase reveal mechanisms of catalysis and of its activation through bicarbonate. *Proc. Natl Acad. Sci. USA* **111**, 3727–3732. (doi:10.1073/pnas.1322778111)
58. Larsen EH, Deaton LE, Onken H, O'Donnell M, Grosell M, Dantzler WH, Weihrauch D. 2014 Osmoregulation and excretion. *Compr. Physiol.* **4**, 405–573. (doi:10.1002/cphy.c130004)
59. Gong F, Alzamora R, Smolak C, Li H, Naveed S, Neumann D, Hallows KR, Pastor-Soler NM. 2010 Vacuolar H^+-ATPase apical accumulation in kidney intercalated cells is regulated by PKA and AMP-activated protein kinase. *Am. J. Physiol. Renal Physiol.* **298**, F1162–F1169. (doi:10.1152/ajprenal.00645.2009)
60. Hallows KR *et al.* 2009 Regulation of epithelial Na^+ transport by soluble adenylyl cyclase in kidney collecting duct cells. *J. Biol. Chem.* **284**, 5774–5783. (doi:10.1074/jbc.M805501200)
61. Paunescu TG, Da Silva N, Russo LM, McKee M, Lu HAJ, Breton S, Brown D. 2008 Association of soluble adenylyl cyclase with the V-ATPase in renal epithelial cells. *Am. J. Physiol. Renal Physiol.* **294**, F130–F138. (doi:10.1152/ajprenal.00406.2007)
62. Galvez F, Reid SD, Hawkings G, Goss GG. 2002 Isolation and characterization of mitochondria-rich cell types from the gill of freshwater rainbow trout. *AJP Regul. Integr. Comp. Physiol.* **282**, R658–R668. (doi:10.1152/ajpregu.00342.2001)
63. Wilson CM, Roa JN, Cox GK, Tresguerres M, Farrell AP. 2016 Introducing a novel mechanism to control heart rate in the ancestral pacific hagfish. *J. Exp. Biol.* **219**, jeb138198. (doi:10.1242/jeb.138198)
64. Ladilov Y, Appukuttan A. 2014 Role of soluble adenylyl cyclase in cell death and growth. *Biochim. Biophys. Acta* **1842**, 2646–2655. (doi:10.1016/j.bbadis.2014.06.034)
65. Espejo MS, Orlowski A, Ibañez AM, Di Mattía RA, Velásquez FC, Rossetti NS, Ciancio MC, De Giusti VC, Aiello EA. 2020 The functional association between the sodium/bicarbonate cotransporter (NBC) and the soluble adenylyl cyclase (sAC) modulates cardiac contractility. *Pflügers Arch. Eur. J. Physiol.* **472**, 103–115. (doi:10.1007/s00424-019-02331-x)
66. Schirmer I *et al.* 2018 Soluble adenylyl cyclase: a novel player in cardiac hypertrophy induced by isoprenaline or pressure overload. *PLoS ONE* **13**, e0192322. (doi:10.1371/journal.pone.0192322)
67. Shiels HA, Galli GLJ. 2014 The sarcoplasmic reticulum and the evolution of the vertebrate heart. *Physiol. Bethesda Md.* **29**, 456–469. (doi:10.1152/physiol.00015.2014)
68. Zippin JH, Farrell J, Huron D, Kamenetsky M, Hess KC, Fischman DA, Levin LR, Buck J. 2004 Bicarbonate-responsive 'soluble' adenylyl cyclase defines a nuclear cAMP microdomain. *J. Cell Biol.* **164**, 527–534. (doi:10.1083/jcb.200311119)
69. Strazzabosco M, Fiorotto R, Melero S, Glaser S, Francis H, Spirli C, Alpini G. 2009 Differentially expressed adenylyl cyclase isoforms mediate secretory functions in cholangiocyte subpopulation. *Hepatol. Baltim. Md.* **50**, 244–252. (doi:10.1002/hep.22926)
70. Tresguerres M, Clifford AM, Harter TS, Roa JN, Theis AB, Yee D, Brauner C. 2020 Evolutionary links between intra- and extracellular acid–base regulation in fish and other aquatic animals. *J. Exp. Zool.* **333**, 449–465. (doi:10.1002/jez.2367)
71. Lee LEJ, Dayeh VR, Schirmer K, Bols NC. 2009 Applications and potential uses of fish gill cell lines: examples with RTgill-W1. *Vitro Cell Dev. Biol. Anim.* **45**, 127–134. (doi:10.1007/s11626-008-9173-2)
72. Fischer M *et al.* 2019 Repeatability and reproducibility of the RTgill-W1 cell line assay for predicting fish acute toxicity. *Toxicol. Sci.* **169**, 353–364. (doi:10.1093/toxsci/kfz057)
73. Schnell S, Stott LC, Hogstrand C, Wood CM, Kelly SP, Pärt P, Owen SF, Bury NR. 2016 Procedures for the reconstruction, primary culture and experimental use of rainbow trout gill epithelia. *Nat. Protoc.* **11**, 490–498. (doi:10.1038/nprot.2016.029)
74. Zippin JH, Chen Y, Nahirney P, Kamenetsky M, Wuttke MS, Fischman DA, Levin LR, Buck J. 2003 Compartmentalization of bicarbonate-sensitive adenylyl cyclase in distinct signaling microdomains. *FASEB J.* **17**, 82–84. (doi:10.1096/fj.02-0598fje)
75. Magro CM, Yang S-E, Zippin JH, Zembowicz A. 2012 Expression of soluble adenylyl cyclase in lentigo maligna: use of immunohistochemistry with anti–soluble adenylyl cyclase antibody (R21) in diagnosis of lentigo maligna and assessment of margins. *Arch. Pathol. Lab. Med.* **136**, 1558–1564. (doi:10.5858/arpa.2011-0617-OA)
76. Zippin JH, Chadwick PA, Levin LR, Buck J, Magro CM. 2010 Soluble adenylyl cyclase defines a nuclear cAMP microdomain in keratinocyte hyperproliferative skin diseases. *J. Invest. Dermatol.* **130**, 1279–1287. (doi:10.1038/jid.2009.440)
77. Watson RL, Buck J, Levin LR, Winger RC, Wang J, Arase H, Muller WA. 2015 Endothelial CD99 signals through soluble adenylyl cyclase and PKA to regulate leukocyte transendothelial migration. *J. Exp. Med.* **212**, 1021–1041. (doi:10.1084/jem.20150354)

Electronic Supplementary Material (ESM) File 1
Supplementary Methods

Fish husbandry

Bamfield Marine Science Center (BC, Canada): mixed sex juvenile steelhead rainbow trout (*Oncorhynchus mykiss*) 100-200 g were purchased from Robertson Creek Fish Hatchery, Port Alberni (BC, Canada) and transported to the Bamfield Marine Science Center, where they were kept in a flow though ~70 L tank supplied with aerated dechlorinated freshwater (pH 7.1, salinity ~0 ppt, 16 °C). Fish were terminally anesthetized with an overdose of tricaine methanesulfonate (1 g/L, MS-222) buffered with $NaHCO_3$, weighed, and perfused through the heart with modified Cortland’s saline (pH 7.85), to remove blood from the tissues (1). Gill, anterior intestine, liver, heart and white muscle were excised and immediately snap frozen in liquid nitrogen and stored in -80 °C for protein analysis. Testis was placed in 500 uL RNA*later* (Sigma-Aldrich, St. Louis, MO, USA) for RNA analysis. This procedure was approved by animal care protocols from the U. of Alberta (AUP00001126 & AUP00000072).

University of Exeter (UK): mixed sex immature rainbow trout (*O. mykiss*) were obtained from Houghton Springs Fish Farm (Houghton, Dorset, UK) and housed at the Aquatic Resources Centre at University of Exeter in 300-400 L stock tanks fed with dechlorinated Exeter city tap water (Na^+ 490, K^+ 47, Ca^{2+} 560, Mg^{2+} 179, Cl^- 495 μmol l^{-1}, pH ~7.7; 15°C). Blood samples were obtained under benzocaine anesthesia as previously described (2). Fish were euthanized by pithing under anesthesia and gill and liver were immediately placed in ice-cold fixative and processed for immunohistochemistry as described previously (3). This procedure was approved by animal care protocols from University of Exeter (PPL P88687E07).

University of Manchester (UK): adult female rainbow trout (*O. mykiss*; ~ 200 g) were purchased from Dunsop Bridge Trout Farm, Ltd (Clitheroe, Lancashire, England). Fish were held in 500 L tanks, with recirculating dechlorinated freshwater (10°C) at U. Manchester. Water quality was checked every second day and water was changed 3 times per week. Fish were killed by concussion of the brain, followed by pithing. Ventricular myocytes were freshly isolated as described previously (4), white muscle was dissected and placed in ice-cold fixative (see below). Fish husbandry and experimental procedures were in accordance with local animal-handling protocols and adhere to the United Kingdom Home Office legislation, and approved by animal care protocols from U. Manchester (HO lic 40/3584).

Immunostaining of myocytes, RBCs, and RTgill-W1 cells

White muscle was fixed in 4% paraformaldehyde overnight at 4°C and stored in 70% ethanol at 4°C for processing. Muscle fibers were carefully separated with two needles and stepwise re-hydrated in 50% ethanol followed by PBS overnight. Tissues were blocked (2% normal goat serum, 0.02% key-hole limpet haemocyanin, and 0.2 % Tween20 in PBS) for 8 hours on a rotator at 4°C. Primary antibodies, anti-rtsAC C1 (1:500) and anti-α-tubulin antibody (1:150) were added directly into the blocking buffer and the tissues were incubate overnight on a rotator at 4°C. The next day, the blocking buffer was decanted and the tissues were rinsed three times with PBS-T (0.2 % Tween20 in PBS) for 5 min on a rotator at room temperature. Detection of the primary antibodies was with a goat anti-rabbit Alexa 555 (1:500), goat anti-mouse IgG conjugated to Alexa 488 (1:500; Invitrogen A28175) and DAPI to visualize the nucleus (1:1000). Tissues were incubated with secondary antibodies for 2 h on a rotator at room temperature. Finally, the blocking buffer was decanted and tissues were washed three times with PBS-T for 5 min on a rotator at room temperature and stored in PBS at 4°C in the dark.

Red blood cells (RBC) were obtained by caudal puncture into heparinized syringes and plasma proteins were removed by centrifuging the RBCs (1,500 xg for 2 min at 4°C, throughout) and re-suspending the pellet in PBS three times. Thereafter, the cells were re-suspended in cold fixative (3% paraformaldehyde and 0.175 % glutaraldehyde in PBS) and incubated for 40 min on a rotator at 4°C. After fixation the cells were rinsed three times in PBS and then permeabilised (0.1% TritonX in PBS) and auto-fluorescence quenched (100 mM glycine in PBS) for 15 min on a rotator at room temperature. The cells were stored in PBS at 4°C in the dark. For IHC the RBCs were blocked (3% bovine serum albumin and 1% normal goat serum in PBS) for 4 h on a rotator at room temperature. The anti-rtsAC C1 primary antibody was added directly into the blocking buffer and incubation was overnight on a rotator at 4°C. The next day the cells were rinsed three times in PBS, re-suspended in blocking buffer with goat anti-rabbit IgG conjugated to Alexa 555 (1:500; Invitrogen A27039) and Hoechst 33342 dye (Invitrogen) to

ESM Table S1. Primers sets used in the RT-PCR experiments and GenBank accession numbers of the rtsAC splice variants. Tm= melting temperature. Primers were designed based on GenBank gene sequences CCAF010022380.1 (1) and MSJN01002537.1 (2).

No. in Figure S3	ID Accession number	Primer sequence (5'-3')	Tm (°C)	Amplicon (bp)
A	**rtsAC$_{FL}$**	**F1** GCTCAACGGAAAACATGATGCC	57.2	
	MF034909	**R1** CGAGATGAAATGATACCAACACTC	53.6	5144
B	**rtsAC$_{T}$**	**F1** *see above*		
	MF034903	**R2** CAATAGTCCAGTCCTCAATATGAAAGT	54.6	1536
C	**rtsAC$_{C1a}$**	**F2** ATGGGTTGGATAAAGGGAGAG	54.0	
	MF034907	**R3** TCTCCTCACACACTCTGTAGAC	55.3	776
D	**rtsAC$_{C1b}$**	**F2** *see above*		
	MF034906	**R4** CCTCAATATGAAAGTGAGTACCAG	52.9	1000
E	**rtsAC$_{C1c}$**	**F1** *see above*		
	MF034908	**R2** *see above*		1715
F	**rtsAC$_{C2}$**	**F1** *see above*		
	MF034905	**R2** *see above*		1249
G, H	**rtsAC$_{43}$ & rtsAC$_{36}$**	**F2** *see above*		
	MF034911	**R3** *see above*		852
G	**rtsAC$_{43}$**	**F6** GTGACAAGAGGTACCGTAACGA	56.2	
	MF034914	**R2** *see above*		1041
H	**rtsAC$_{36}$**	**F6** *see above*		
	MF034913	**R2** *see above*		858
I	**rtsAC$_{37}$**	**F1** *see above*		
	MF034915	**R12** AGCAGATATACCTGAGACATCCGC	58.1	206
		F7 CGGATGTCTCAGGTATATCTGCTG	56.5	
	MF034916	**R2** *see above*		1244
J		**F4** TGGGTTGGATAAAGGGAGAGG	56.2	
	MF034910	**R6** TTGTCCCGCTCACATAGTTCC	57.0	505
K		**F1** *see above*		
	MF034917	**R7** GGTCCATGAGTGACACATCTTTC	55.6	1762
L		**F1** *see above*		
	MF511189	**R8** CAGACTCTTGTACGTTGAGCAAAC	56.0	2829
M		**F3** CATCAACATCCTGCCAGAGTC	55.6	
	MF034927	**R5** CTAGGCTACCTTCTGTGTGC	55.0	692
N		**F5** GTGTAGTAGGACATCCAGTGAG	54.1	
	MF034922	**R9** GCATACCACAGAGCCAGAG	55.3	2623
O		**F1** *see above*	57.2	
	MF034920	**R10** GAGTCGTGCAGGTGGTCTA	56.4	2621
		F5 *see above*		
	MF034921	**R9** *see above*		1744
P		**F1** *see above*	57.2	
	MF034918	**R11** CGATGGAGAGGAGGACTCTC	56.0	1813
		F5 *see above*		
	MF034919	**R9** *see above*		967
Q		**F5** *see above*		
	MF034923	**R9** *see above*		943
R		**F3** *see above*		
	MF034925	**R5** *see above*		1960
S		**F5** *see above*		
	MF034924	**R9** *see above*		2108
T		**F8** *see above*		
	MF034926	**R8** *see above*		737
	rtef1α	**F** TCCTCTTGGTCGTTTCGCTG	57.4	159
	AF498320	**R** ACCCGAGGGACATCCTGTG	59.2	

1. Berthelot C, Brunet F, Chalopin D, Juanchich A, Bernard M, Noël B, et al. The rainbow trout genome provides novel insights into evolution after whole-genome duplication in vertebrates. Nature communications. 2014 Apr;5:3657.
2. Lien S, Gao G, Baranski M, Moen T, Nome T, Miller M, et al. A new and improved rainbow trout (*Oncorhynchus mykiss*) reference genome assembly. In 2016. p. 40.

visualize the nucleus (1:1000), for 2 h on a rotator at room temperature. Finally, the cells were rinsed three times in PBS and stored at 4°C in the dark.

RTgill-W1 cells grown in glass bottom collagen coated culture dishes were fixed (3.7% paraformaldehyde in PBS, 10 min) rinsed with PBS, permeabilized with 0.5% Triton X-100 in PBS for 5 min, and rinsed again with PBS. Cells were then incubated with blocking buffer (10 mg/mL BSA in PBS) for 1 h and incubated with primary antibodies diluted in blocking buffer (4°C, overnight). Anti-rtsAC-C1, anti-rtsAC-FL, anti-α-tubulin were applied at 1:1000 dilution,anti-GM130 was applied at 1:100 dilution. On the following day, cells were washed (3x in PBS) and then incubated with secondary antibodies (1:500 in PBS) in the dark. After washing in PBS (3x), nuclei were stained with Hoechst 33342 dye (1:1,000 dilution in PBS) for 5 min. Cells were washed (3x, PBS) and kept submerged in PBS. Mitochondria were visualized by incubating cells with 200 nM MitoTracker Orange CMTMRos (Invitrogen) diluted in PBS for 25 min at 18°C before fixation. Ventricular myocytes were processed in a similar manner to RTgill-W1 cells. Mouse anti-sarcomeric α-actinin (EA-53) (abcam, Cambridge, MA, USA) was applied at 1:200 dilution.

1. Wolf K. Physiological Salines for Fresh-Water Teleosts. The Progressive Fish-Culturist. 1963 Jul;25(3):135–40.
2. Montgomery DW, Simpson SD, Engelhard GH, Birchenough SNR, Wilson RW. Rising CO_2 enhances hypoxia tolerance in a marine fish. Sci Rep. 2019 Dec;9(1):15152.
3. Roa JN, Tresguerres M. Bicarbonate-sensing soluble adenylyl cyclase is present in the cell cytoplasm and nucleus of multiple shark tissues. Physiological Reports. 2017;24:e13090.
4. Shiels HA, Vornanen M, Farrell AP. Temperature-dependence of L-type Ca^{2+} channel current in atrial myocytes from rainbow trout. J Exp Biol. 2000 Sep;203(Pt 18):2771–80.

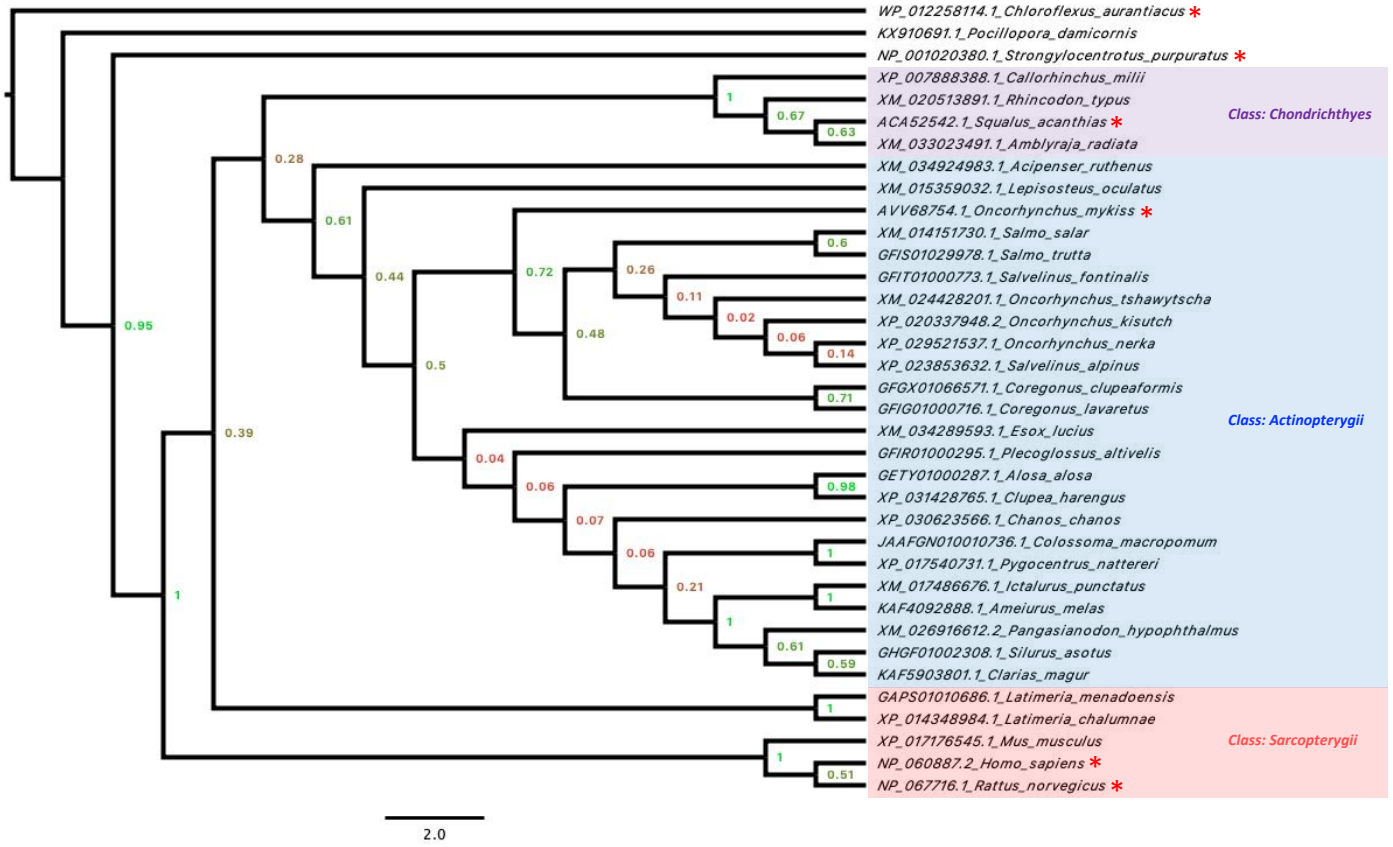

Figure S1. Phylogenic analysis of sAC ortholog proteins in fishes. The tree was constructed using the "*A la carte*" analysis in www.*Phylogeny.fr* using MUSCLE to align the sequences (16 maximum number of iterations; "Find diagonals": enabled), followed by Gblocks curation and tree reconstruction using the maximum likelihood method using default parameters and 100 bootstrap replicates to assess reliability of internal branches. The tree was drawn using FigTree (http://tree.bio.ed.ac.uk/). Bootstrap values are provided for the nodes following a color gradient scheme ranging from green for high values to red for low values. The scale bar represents substitutions per amino acid site. Each sequence name starts with its GenBank accession number followed by *Genus_species*. Nucleotide sequences were translated to amino acid sequences. The red asterisks indicate sAC sequences experimentally confirmed to be stimulated by HCO_3^-. Common species names can be found in Table S2.

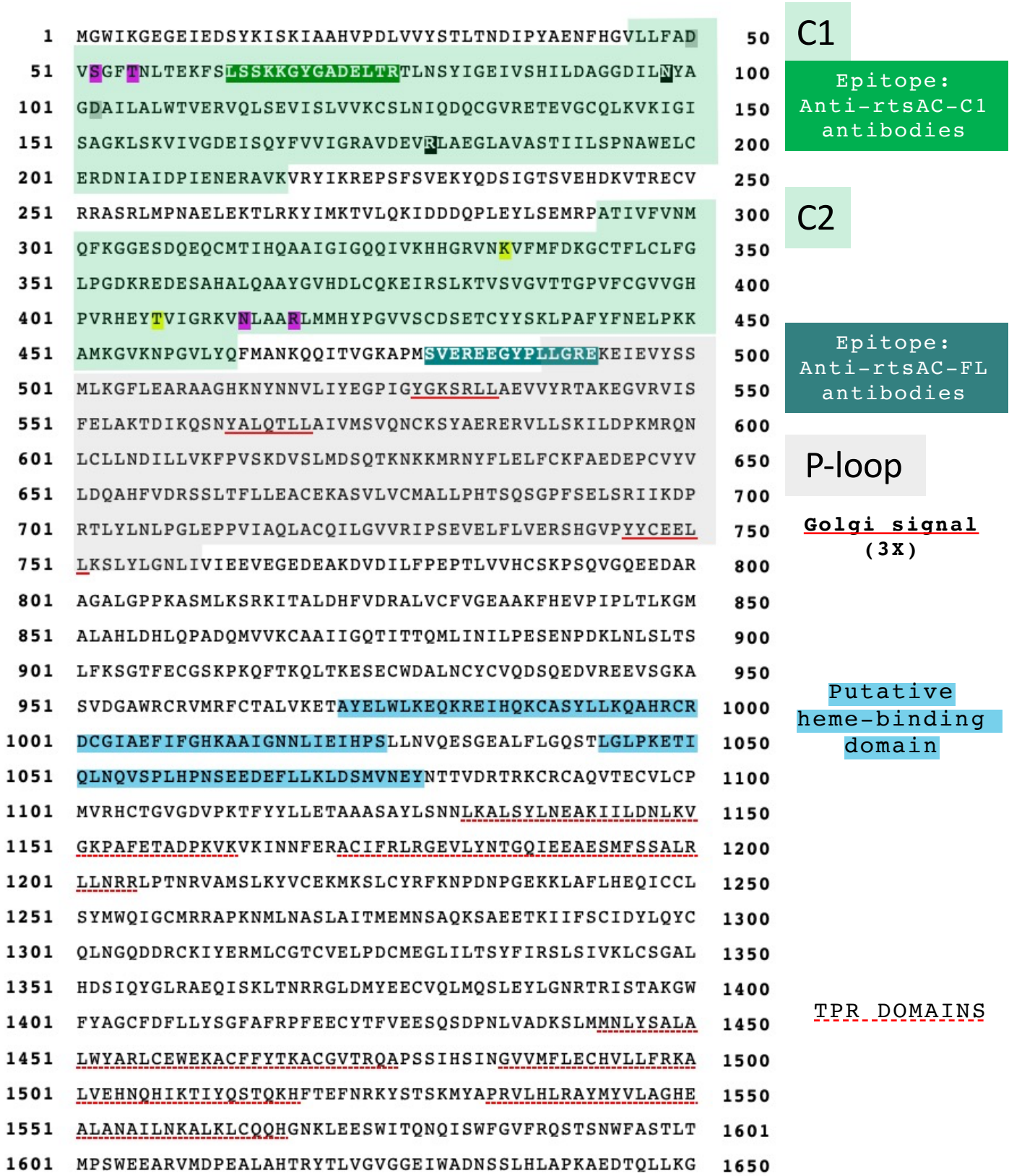

Figure S2. Amino acid sequence and topology of rtsAC$_{FL}$. Predicted molecular architecture of rtsAC$_{FL}$ (GenBank accession no. MF034909). Catalytic domains C1 and C2 are highlighted in light green. The P-loop domain is highlighted in grey. Three Golgi apparatus targeting sequences in the P-loop domain are underlined in red. Five Tetratricopeptide repeat (TPR)-like domains are underlined in dashed red lines. The epitope recognized by anti-rtsAC-C1 antibodies is highlighted in dark green, and the epitope recognized by anti-rtsAC-FL antibodies is highlighted in teal. The putative heme-binding domain is highlighted in blue. The two conserved aspartate residues (D50 and D102) that bind two divalent cations and contribute to ATP binding and turnover are highlighted in grey. Arginine 418 (R418), serine 52 (S52), threonine 55 (T55) and asparagine 414 (N414), which interact with the different phosphates of the ATP molecule, are highlighted in magenta. Lysine 335 (K335) and threonine 407 (T407), which bind to adenine in the ATP molecule, are highlighted in yellow. Asparagine 98 (N98) and arginine 179 (R179), which presumably bind HCO_3^-, are highlighted in black. Notice that N98 is different from the equivalent human sAC residue (which is a lysine, K95) (see reference 14). The features are based on mammalian sAC (references 2–5).

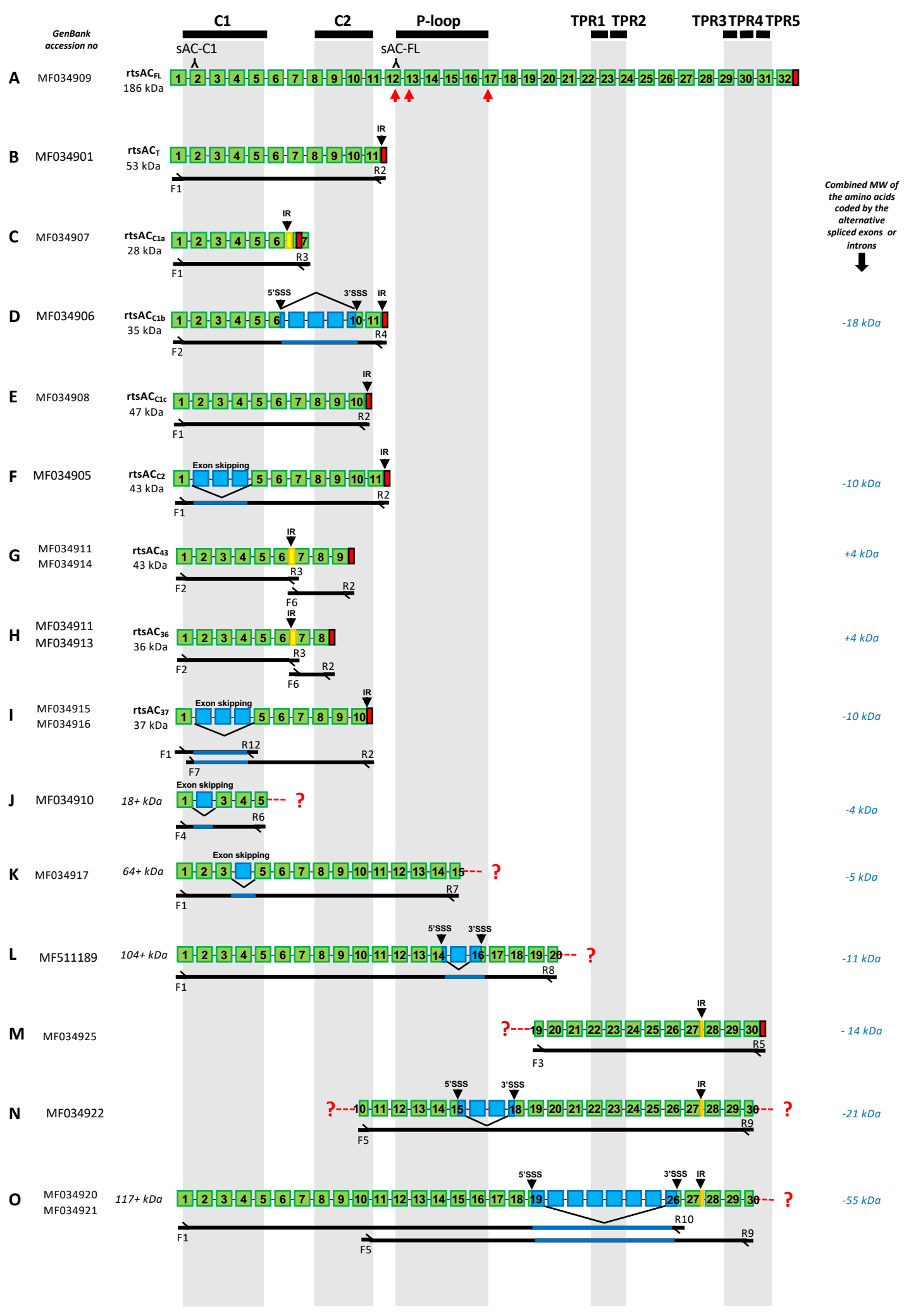
GenBank accession no
C1
C2
P-loop
TPR1 TPR2
TPR3 TPR4 TPR5
sAC-C1
sAC-FL
A MF034909 rtsAC$_{FL}$ 186 kDa
B MF034901 rtsAC$_{T}$ 53 kDa
C MF034907 rtsAC$_{C1a}$ 28 kDa
D MF034906 rtsAC$_{C1b}$ 35 kDa
E MF034908 rtsAC$_{C1c}$ 47 kDa
F MF034905 rtsAC$_{C2}$ 43 kDa
G MF034911 MF034914 rtsAC$_{43}$ 43 kDa
H MF034911 MF034913 rtsAC$_{36}$ 36 kDa
I MF034915 MF034916 rtsAC$_{37}$ 37 kDa
J MF034910 18+ kDa
K MF034917 64+ kDa
L MF511189 104+ kDa
M MF034925
N MF034922
O MF034920 MF034921 117+ kDa
IR
5'SSS
3'SSS
Exon skipping
F1
F2
F3
F4
F5
F6
F7
R2
R3
R4
R5
R6
R7
R8
R9
R10
R12
Combined MW of the amino acids coded by the alternative spliced exons or introns
-18 kDa
-10 kDa
+4 kDa
+4 kDa
-10 kDa
-4 kDa
-5 kDa
-11 kDa
- 14 kDa
-21 kDa
-55 kDa

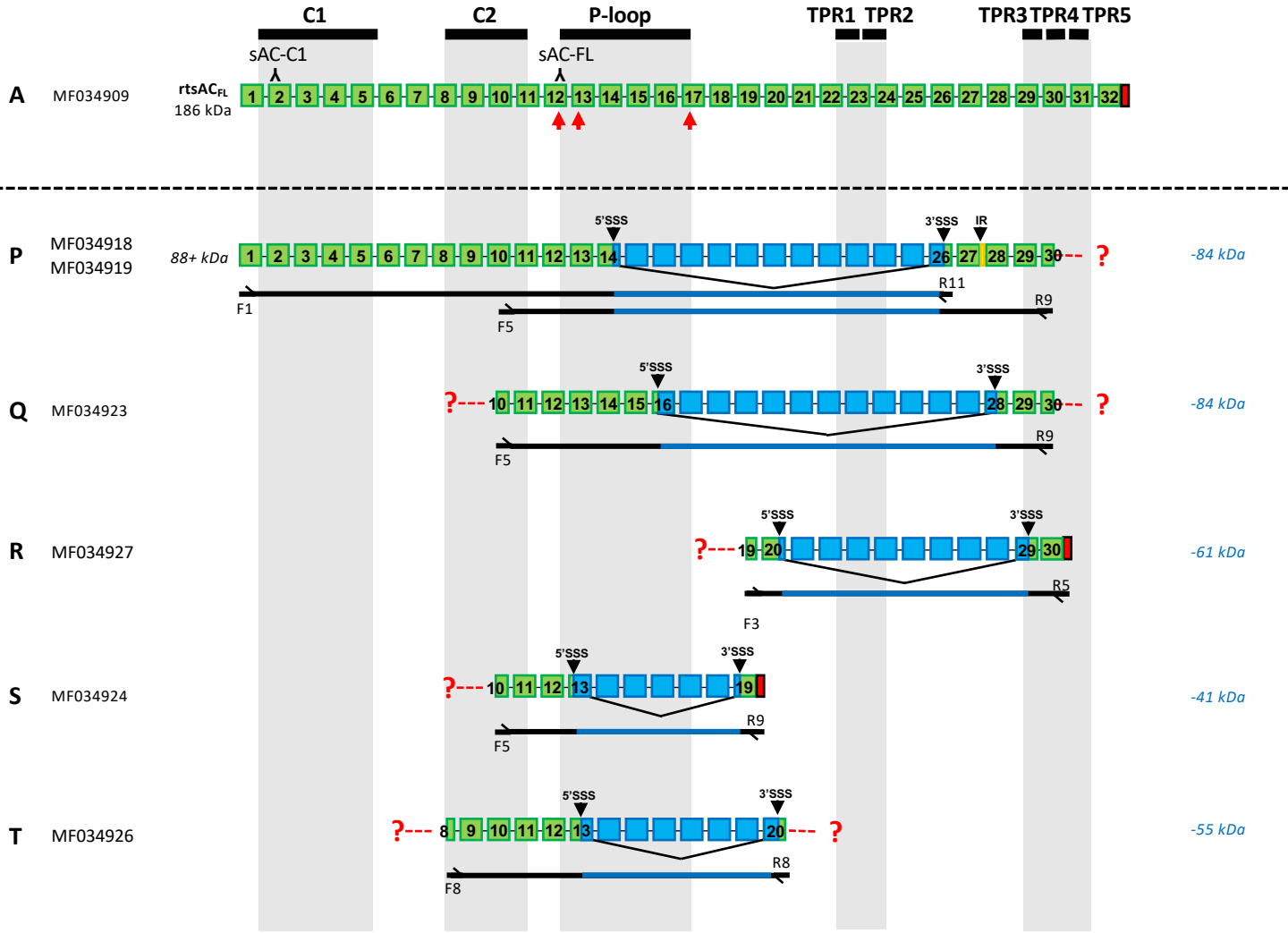

Figure S3. Schematic organization of rtsAC isoforms. *Complete Open Reading Frame (ORF):* rtsAC A-F. *Incomplete ORF:* rtsAC G-T. C1 and C2: catalytic domains; Green boxes: exons; Red boxes: contain stop codons; Blue boxes: skipped exons; Inverted (Y): epitopes recognized by anti-sAC-C1 and anti-sAC-FL antibodies; P-loop: P-loop domain; TRP: tetratricopeptide repeat (TPR)-like domain (1 to 5); IR: intron retention. 3' and 5'SSS: alternative 3' or 5' splice site selection. The red arrows in (A) indicate Golgi apparatus targeting sequences. The black arrows indicate the primer sets used to clone each sequence (F= forward; R= Reverse) and are listed in Table S1 (Electronic Supplemental Material).

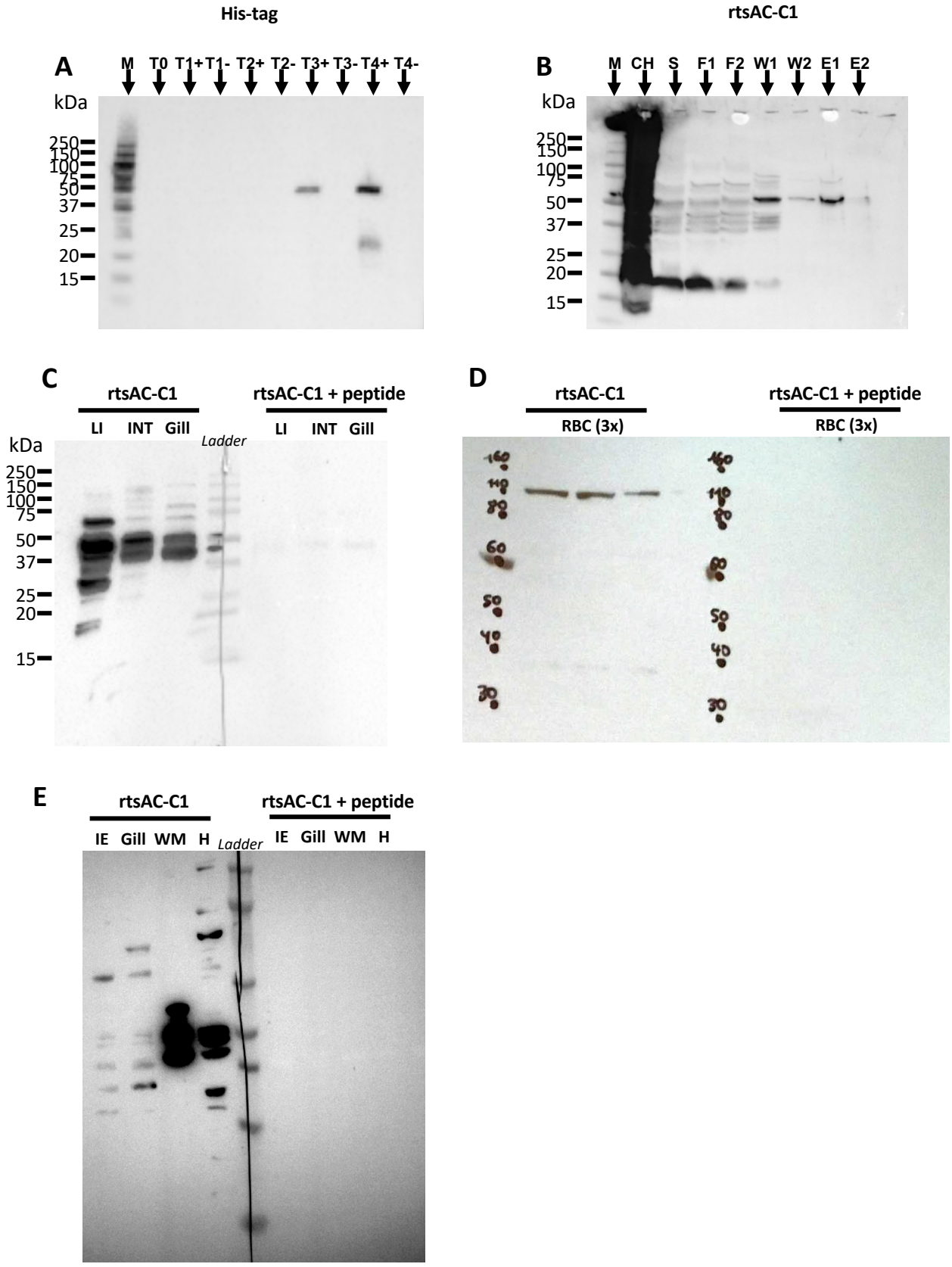

Figure S4. Production and purification of His-rtsAC$_T$ and anti-rtsAC$_T$ antibody validation. (A) Western blot detection of His-rtsAC$_T$ protein using a monoclonal anti-His-tag antibody in the insoluble fraction of BL21-AI One Shot bacteria induced with 0.2% L-arabinose (+) or uninduced (-) at Time= 0, 1, 3 and 4 h. **(B)** Western blot detection of His-rtsAC$_T$ protein using anti-rtsAC-C1 antibodies in different fractions through the protein purification process through Ni-NTA resin and eluted with 5 mL PBS with 250mM imidazole; pH 7.4 (His-rtsAC$_T$ was produced in bacteria induced with 0.2% L-arabinose for 3 h CH: crude homogenate; S: soluble fraction; F1 and 2: flow-through 1 and 2; W1 and 2: wash 1 and 2; E1 and 2: elution 1 and 2). Western blot peptide preabsorption controls for the anti-rtsAC-C1 antibodies in trout **(C)** liver [LI], intestine [INT] and gill; **(D)** red blood cells (RBCs) (samples from three different trout); and **(E)** inner ear [IE], gill, white muscle (WM), and heart (H).

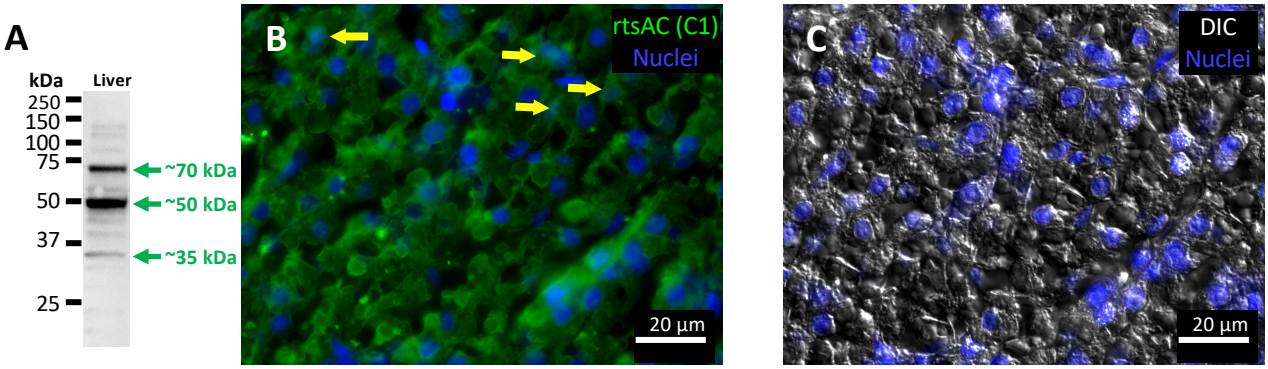

Figure S5. Presence and localization of rtsAC protein in trout liver cells. (A) Western Blot of liver tissue probed with anti-rtsAC-C1 antibodies detected three main bands ranging from ~35 to ~70 kDa. **(B)** Liver tissue immunostained anti-rtsAC-C1 antibodies (green). Yellow arrows indicate nuclear staining. **(C)** Corresponding pre-absorption peptide control in which the anti-rtsAC-C1 antibodies were pre-incubated with 3X excess corresponding antigen peptide with image merged with differential interference contrast (DIC). Nuclei were labeled with Hoechst 33342 (blue). Scale bars = 20 μm.

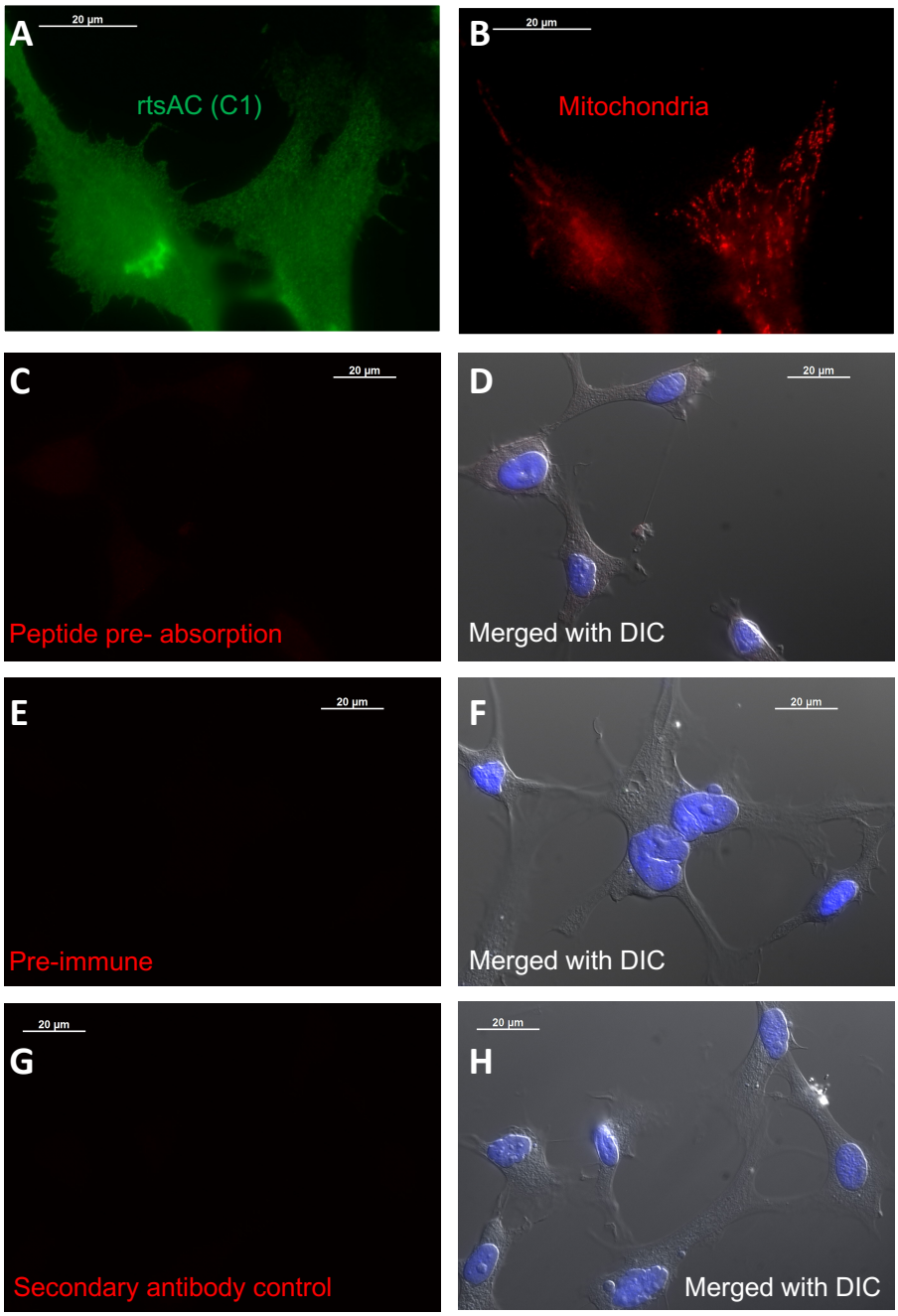

Figure S6. Figure S6. Immunocytochemistry analysis of RTgill-W1 cells. Immunofluorescent staining of RTgill-W1 cells using: **(A)** anti-rtsAC-C1 antibodies (green) and **(B)** mitochondria (MitoTracker) (red). **(C)** Pre-absorption peptide control in which the anti-rtsAC-C1 antibodies were pre-incubated with 3X excess corresponding antigen peptide (red). **(D)** Image C merged with the corresponding differential interference contrast (DIC) image. **(E)** Pre-immune serum control incubating (serum from the rabbit that produce the anti-rtsAC-C1 antibodies, before immunization) (red). **(F)** Image E merged with the corresponding DIC image. **(G)** Secondary antibody control (sections incubated without primary antibodies) (red). **(H)** Image G merged with the corresponding DIC image. Nuclei were labeled with Hoechst 33342 (blue). Scale bars = 20 μm.

ESM Table S2. Accession numbers for the sAC sequences from ray-finned (Actinopterygii) organized in taxonomic ranks. WGS= whole genome shotgun. TSA= transcriptomic shotgun assembly. MW= molecular weight. Sequences were obtained from NCBI (https://www.ncbi.nlm.nih.gov/) and The Ensembl project (http://www.ensembl.org/), supplemented by information found in (1–4). Fish taxonomy was based on (5). The species and sequences in **bold** were used to construct the phylogenetic tree in figure S1.

GenBank or Ensembl # (Type of database) [Tissue] (predicted MW)	Species	Order	Superorder	Infraclass	Subclass
GGZX01444657.1; GEUL01120300.1 (TSA) [multiple pooled tissues] (short sequences, partial)	Atlantic sturgeon (*Acipenser oxyrinchus*)	Acipenseriformes			Chondrostei
GICD01020348.1 (TSA) [male and female gonads] (short sequence, partial)	Siberian sturgeon (*A. baerii*)				
GGYF01100418.1; GGYF01032689.1; GGYF01032688; GGYF01107205.1 (TSA) (multiple pooled tissues) (short sequences, partial)	Chinese sturgeon (*A. sinensis*)				
XM_034924983.1 (WGS) (187 kDa); RXM28897.1 (WGS) (134 kDa)	**Sterlet sturgeon (*A. ruthenus*)**				
XM_015359032.1 (WGS, supported by mRNA from unspecified tissue) (190 kDa)	**Gar (*Lepisosteus oculatus*)**	Lepisosteiformes		Holostei	Neopterygii
XM_014151728.1 (TSA) [muscle] (188 kDa); XM_014151729.1 (TSA) [muscle] (172 kDa); XM_014151730.1 (TSA)[muscle] (172 kDa); XM_014151731.1 (TSA) [muscle] (160 kDa); GEGX01191412.1 (TSA)[testis] (188 kDa); GEGX01191405.1 (TSA) [testis] (187 kDa); GEGX01191400.1 (TSA) [testis] (172 kDa); GEGX01191404.1 (TSA) [testis] (172 kDa); GEGX01191417.1 (TSA) [testis] (168 kDa); GEGX01191402.1 (TSA) [testis] (162 kDa); GBRB01066503.1 (TSA) [reference transcript from multiple tissues] (172 kDa); NW_012338874.1 (WGS)	**Atlantic salmon (Salmo salar)**	Salmoniformes	Protacanthopterygii	Teleostei	
GFIS01029978.1 (TSA) [multiple pooled tissues] (93 kDa)	**Brown trout (*Salmo trutta*)**				
This study (Table S1) rtsAC$_T$ protein sequence used in the tree**: AVV68754.1**	**Rainbow trout (*Oncorhynchus mykiss*)**				
XM_024428201.1 (TSA) [fin] (180 kDa)	**Chinook salmon (*Oncorhynchus tshawytscha*)**				
XP_020337948.2 (WGS) (186 kDa); XM_020482359.1 (TSA) [muscle] (91 kDa, contains stop codon);); XM_020482359.1 (updated version; 186 kDa)	**Coho salmon (*O. kisutch*)**				
XP_029521537.1 (TSA) [caudal fin] (188 kDa)	**Sockeye salmon (*Oncorhynchus nerka*)**				
QNTS01000485.1; QNTS01000812.1 (WGS)	Danube salmon (*Hucho hucho*)				
GFIT01000773.1 (TSA) [multiple pooled tissues] (168 kDa, incomplete)	**Brook trout (*Salvelinus fontinalis*)**				
XP_023853632.1 (TSA) [liver] (163 kDa)	**Arctic char (*S. alpinus*)**				
GFIG01000716.1 (TSA) [multiple pooled tissues] (188 kDa)	**European whitefish (*Coregonus lavaretus*)**				
GFGX01066571.1 (TSA) [multiple pooled tissues] (188 kDa)	**American whitefish (*C. clupeaformis*)**				
GFIZ01000614.1 (TSA) [multiple pooled tissues] (160 kDa; missing C1); GFVB01035058.1, GFVB01013412.1, GFVB01136541.1 (TSA) [Embryo, fry] (short sequences, partial)	Grayling (*Thymallus thymallus*)				
XM_034289593.1 (TSA) [liver and spleen] (180 kDa); XM_020042476.1 (TSA) [spleen] (125 kDa); XM_020042477.1 [spleen] (117 kDa); XM_020042478.1 [spleen] (109 kDa); XM_020042479.1 [spleen] (107 kDa); AZJR03000177.1 (WGS)	**Northern pike (*Esox lucius*)**	Esociformes			
GFIR01000295.1 (TSA) [multiple pooled tissues] (190 kDa)	**Ayu (*Plecoglossus altivelis*)**	Osmeriformes			
OMKJ01051719.1 (WGS)	European smelt (*Osmerus eperlanus*)				
XM_017486676.1 (TSA) [blood] (146 kDa); XM_017486692.1 (TSA) [blood] (138 kDa)	**Channel catfish (*Ictalurus punctatus*)**	Siluriformes	Ostariophysi		
XM_026916612.2 (TSA) [blood] (146 kDa); XM_026918889.1 (TSA) [blood] (136 kDa) [testis]	**Shark catfish (*Pangasius hypophthalmus*)**				
QMIH01000557.1 (WGS)	Walking catfish (*Clarias batrachus*)				
KAF5903801.1 (WGS)	**Walking catfish (*C. magur*)**				

GHGF01002308.1 (TSA) [multiple pooled tissues] (146 kDa) (short sequence, partial)	**Amur catfish (*Silurus asotus*)**				
KAF4092888.1 (WGS) (147 kDa)	**Black bullhead catfish (*Ameiurus melas*)**				
GDHW01207338.1 (TSA) [whole embryo]	Annual killifish (*Austrofundulus limnaeus*)	Cypriniformes			
XP_017540731.1 (TSA) [unspecified tissue, female] (186 kDa); MAUM01030526.1 (WGS)	**Piranha (*Pygocentrus nattereri*)**	Characiformes			
JAAFGN010010736.1 (WGS).	**Tambaqui (*Colossoma macropumum*)**				
XP_030623566.1 (WGS) (186 kDa)	**Milkfish (*Chanos chanos*)**	Gonorynchiformes			
XP_031428765.1 (WGS) (194 kDa); XM_012838322.1 [mRNA from unspecified tissue] (92 kDa)	**Herring (*Clupea harengus*)**	Clupeiformes	Clupeomorpha		
QPKT01024983.1 (WGS); UIGZ01009659.1 (WGS); UIGZ01023758.1 (WGS); QPKT01030036.1 (WGS); UIGZ01013918.1 (WGS); HAMD01025856 (mRNA) [unspecified tissue, female) (short sequence, partial); HAMA01162168. (mRNA) [unspecified tissue, female) (short sequence, partial)	European plichard (*Sardina pilchardus*)				
QYSC01119099.1 (WGS); QYSC01026046.1 (WGS); QYSC01033477.1 (WGS); QYSC01025067.1 (WGS)	Ilish (*Tenualosa ilisha*)				
GETY01000287.1 (TSA) [multiple pooled tissues]	**Allis shad (*Alosa alosa*)**				
OOFF01048719.1 (WGS); OOFF01071954.1 (WGS); OOFF01081955.1 (WGS); OOFF01081981.1 (WGS)	Snaggletooth (*Borostomias antarcticus*)	Stomiiformes	Stenopterygii		

1. Lien S, Gao G, Baranski M, Moen T, Nome T, Miller M, et al. A new and improved rainbow trout (*Oncorhynchus mykiss*) reference genome assembly. In 2016. p. 40.
2. Berthelot C, Brunet F, Chalopin D, Juanchich A, Bernard M, Noël B, et al. The rainbow trout genome provides novel insights into evolution after whole-genome duplication in vertebrates. Nature communications. 2014 Apr;5:3657.
3. Kaitetzidou E, Ludwig A, Gessner J, Sarropoulou E. Expression Patterns of Atlantic Sturgeon (*Acipenser oxyrinchus*) During Embryonic Development. G3. 2017 Feb;7(2):533–42.
4. Leong JS, Jantzen SG, von Schalburg KR, Cooper GA, Messmer AM, Liao NY, et al. Salmo salar and Esox lucius full-length cDNA sequences reveal changes in evolutionary pressures on a post-tetraploidization genome. BMC Genomics. 2010;11(1):279.
5. Pasquier J, Cabau C, Nguyen T, Jouanno E, Severac D, Braasch I, et al. Gene evolution and gene expression after whole genome duplication in fish: the PhyloFish database. BMC Genomics. 2016 Dec;17(1):368.